



# AMERICAN METEOROLOGICAL SOCIETY

*Monthly Weather Review*

## **EARLY ONLINE RELEASE**

This is a preliminary PDF of the author-produced manuscript that has been peer-reviewed and accepted for publication. Since it is being posted so soon after acceptance, it has not yet been copyedited, formatted, or processed by AMS Publications. This preliminary version of the manuscript may be downloaded, distributed, and cited, but please be aware that there will be visual differences and possibly some content differences between this version and the final published version.

The DOI for this manuscript is doi: 10.1175/MWR-D-16-0102.1

The final published version of this manuscript will replace the preliminary version at the above DOI once it is available.

If you would like to cite this EOR in a separate work, please use the following full citation:

Fine, C., R. Johnson, P. Ciesielski, and R. Taft, 2016: The Role of Topographically Induced Vortices in Tropical Cyclone Formation over the Indian Ocean. *Mon. Wea. Rev.* doi:10.1175/MWR-D-16-0102.1, in press.

© 2016 American Meteorological Society



# **The Role of Topographically Induced Vortices in Tropical Cyclone**

## **Formation over the Indian Ocean**

Caitlin M. Fine, Richard H. Johnson\*, Paul E. Ciesielski, and Richard K. Taft

*Department of Atmospheric Science, Colorado State University, Fort Collins, Colorado*

PRELIMINARY ACCEPTED VERSION

<sup>5</sup> \* *Corresponding author address:* Richard H. Johnson, Department of Atmospheric Science, 1371

<sup>6</sup> Campus Delivery, Colorado State University, Fort Collins, CO 80523.

<sup>7</sup> E-mail: johnson@atmos.colostate.edu

## ABSTRACT

8 The role of Sumatra and adjacent topographic features in tropical cyclone  
9 (TC) formation over the Indian Ocean (IO) is investigated. Sumatra, as well as  
10 the Malay Peninsula and Java, have mountainous terrain that partially blocks  
11 low-level flow under typical environmental stratification. For easterly low-  
12 level flow, these terrain features often produce lee vortices, some of which  
13 subsequently shed and move westward from the northern and southern tips  
14 of Sumatra and thence downstream over the IO. Since Sumatra straddles the  
15 equator, extending in a northwest-to-southeast direction from approximately  
16  $6^{\circ}\text{N}$  to  $6^{\circ}\text{S}$ , the lee vortices, while counter-rotating, are both cyclonic. Hence,  
17 they can serve as initial disturbances that eventually contribute to TC forma-  
18 tion over the IO. In addition, low-level, equatorial westerly flow impinging  
19 on Sumatra is also typically blocked and diverges, at times contributing to cy-  
20 clonic circulations over the IO, primarily near the southern end of the island.

21 Data from two recent tropical campaigns, the 2008-10 Year of Tropical  
22 Convection (YOTC) and the 2011 Dynamics of the Madden-Julian Oscilla-  
23 tion or MJO (DYNAMO), are used to study these phenomena. These data  
24 sets reveal the frequent occurrence of shed and non-shed terrain-induced cy-  
25 clonic circulations over the IO, the majority of which occur during boreal fall  
26 and winter. During the 2.5 years of the two campaigns, 13 wake vortices (13%  
27 of the shed circulations identified) were tracked and observed to subsequently  
28 develop into TCs over the northern and southern IO, accounting for 25% of  
29 the total TCs forming in the IO during that period.

## 30 **1. Introduction**

31 A number of processes, acting singly or in concert, have been observed to contribute to tropical  
32 cyclone (TC) formation, e.g., African Easterly Waves (AEWs), convectively coupled equatorial  
33 waves, breakdown of the intertropical convergence zone (ITCZ), monsoon troughs, and upper-  
34 level troughs. It has also been proposed that topographic effects may influence TC formation.  
35 This possibility has been explored for the eastern Pacific Ocean by Farfán and Zehnder (1997)  
36 and Zehnder et al. (1999). These studies found that easterly flow impinging upon zonally and  
37 diagonally oriented mountain ranges in Central America and Mexico can generate along-mountain  
38 jets and lee vortices. These features then combine with AEWs and moist flow out of the ITCZ to  
39 initiate tropical cyclogenesis. This paper investigates another possible topographic influence on  
40 TC formation, namely, the generation of vortices by the large cross-equatorial island of Sumatra  
41 and neighboring topographic features, a phenomenon originally proposed by Kuettner (1989).

### 42 *a. Terrain-induced circulations: roles of Sumatra and surrounding topography*

43 When stratified flow is blocked by an isolated obstacle, counter-rotating vortices may form in its  
44 wake as flow diverts to either side of the barrier and converges downstream (Smolarkiewicz and  
45 Rotunno 1989; Rotunno and Smolarkiewicz 1991). When the Froude number ( $U/Nh$ , where  $U$   
46 is the approaching wind speed,  $N$  the Brunt Väisälä frequency, and  $h$  the obstacle height) is less  
47 than one, flow blocking is preferred. Generally, flow will be split or blocked below some criti-  
48 cal height, and will flow over the obstacle above that critical height (Smolarkiewicz and Rotunno  
49 1989). There can be a production of potential vorticity in the wake vortices if the flow surmounting  
50 the barrier undergoes a hydraulic jump, along with an associated slight reduction in the surface  
51 pressure (Schär and Smith 1993a; Epifanio and Durran 2002; Epifanio 2003). For elongated bar-  
52 riers such as Sumatra, wave breaking, flow splitting, and the development of lee vortices depend

53 not only on the Froude number (the inverse of which is the non-dimensional mountain height) but  
54 also on the horizontal aspect ratio of the barrier (the ratio of the cross-stream length scale to the  
55 stream-wise length scale of the barrier) (Smith 1989; Epifanio 2003). For typical flow conditions  
56 around many islands in the tropics and subtropics, lee vortices are commonplace. These vortices  
57 often shed and move downstream as a result of boundary layer separation, perturbations in the  
58 flow, or instability in the wake (Etling 1989; Schär and Smith 1993b). Sumatra is one such island  
59 where the conditions for flow splitting and lee vortex formation are met.

60 In this study it is proposed that flow blocking and splitting by the topography on the island of  
61 Sumatra and adjacent topographic features – the mountainous west end of Java and the Malay  
62 Peninsula – can lead to eventual TC genesis in the Indian Ocean. In this region, the mean flow  
63 impacting the terrain features is principally monsoonal, with easterlies in the winter hemisphere  
64 and westerlies in the summer hemisphere. With respect to Sumatra, a narrow mountain range  
65 stretches along its entire length, from approximately 6°N to 6°S, exceeding 3000 m in elevation  
66 near the island’s northern tip (Fig. 1). Easterly wind blocked by the island will result in wake  
67 vortices over the Indian Ocean in each hemisphere that will rotate in opposite directions, but since  
68 the island straddles the equator, both are cyclonic. This unique situation is not found elsewhere  
69 in the tropics. It is proposed that these wake vortices may then serve as pre-existing cyclonic  
70 disturbances out of which TCs may develop. Such a possibility was first explored by Kuettner  
71 and Soules (1967) and Kuettner (1989), who argued that the splitting of *easterly* flow by Sumatra  
72 was responsible for sets of twin cyclones in the Indian Ocean and, using satellite imagery, traced  
73 these TCs back to wake vortices observed downstream of Sumatra under low-level easterly flow  
74 regimes.

75 However, it is evident from Fig. 1 that for easterly flow there are other islands and topographic  
76 features in the maritime continent that can potentially have an impact on the circulation down-

77 stream over the Indian Ocean. As it turns out, the features other than Sumatra of greatest signif-  
78 icance with respect to lee vortex generation affecting the Indian Ocean are the Malay Peninsula  
79 and the island of Java. For the Malay Peninsula, it will be seen that easterly flow directed around  
80 the Titiwangsa Mountains in the south and across the narrow island gap to the north can lead to lee  
81 vortices that impinge upon or skirt the north end of Sumatra. On the other hand, southeasterly flow  
82 impinging on the high terrain of west Java also leads to the generation of lee vortices downstream,  
83 which upon shedding then pass the southern tip of Sumatra.

84 *Westerly* flow impinging on Sumatra may also result in downstream wake vortices, but these  
85 are both anticyclonic and occur over the islands and inland seas of the maritime continent, so  
86 TC formation related to this flow blocking situation is not a possibility. However, given the high  
87 terrain all along the western side of Sumatra (Fig. 1), blocking of equatorial westerly flow by the  
88 barrier may also contribute cyclonic circulations *upstream* of the island as the flow splits near  
89 the equator and moves north and south. This topographic effect will be seen to be yet another  
90 factor in TC formation over the Indian Ocean, thus expanding upon the idea originally advanced  
91 by Kuettner (1989) regarding the blocking of low-level easterly flow by the island. There have  
92 been previous studies of the blocking of westerly flow by Sumatra in the context of the passage  
93 of the MJO (Inness and Slingo 2006; Wu and Hsu 2009) and convectively coupled Kelvin waves  
94 (Ridout and Flatau 2011) over the maritime continent.

#### 95 *b. Other factors influencing the formation of tropical cyclones*

96 The potential for intensification of terrain-induced vortices into TCs over the eastern Indian  
97 Ocean is affected by seasonal and intraseasonal variability of the flow. As noted, easterly wind  
98 impinging upon Sumatra may be blocked and generate cyclonic lee vortices in both hemispheres.  
99 One source of low-level easterly wind in the Indian Ocean is the Madden-Julian Oscillation (MJO:

100 Madden and Julian 1971, 1972), which is the dominant mode of intraseasonal tropical variability  
101 (e. g., Zhang 2005). In the Indian and western Pacific Oceans, the MJO is characterized by low-  
102 level easterly winds preceding the arrival of an eastward-propagating convective envelope or active  
103 phase, followed by low-level westerly winds. Wake vortices developing over the Indian Ocean  
104 downstream of Sumatra in the easterly flow, once shed, may then traverse an environment with  
105 enhanced moisture and divergence aloft, thus aiding TC genesis. Recently, Duvel (2015) showed  
106 that the MJO enhances the frequency of TC genesis over the southern Indian Ocean by increasing  
107 both the number of tropical depression initiations and the probability of their intensification. The  
108 increased frequency is attributed to the MJO enhancing the cyclonic meridional shear of the zonal  
109 wind in the TC genesis latitudes.

110 The Southeast Asian and Australian monsoons also exert an influence on tropical cyclogenesis  
111 in the Indian Ocean basin. When the summer and winter monsoons are established, strong vertical  
112 wind shear discourages tropical cyclogenesis (Gray 1968). During the transition period into the  
113 winter monsoon, the vertical shear is reduced so that when the low-level flow is easterly, cyclonic  
114 vortices that develop over the Indian Ocean west of Sumatra have a greater opportunity for eventual  
115 intensification into a TC. Indeed, in the limited years that he analyzed, Kuettner (1989) observed  
116 TCs intensifying out of wake vortices generated by Sumatra between October and December, and  
117 in May, which represent the monsoon transition periods.

118 Synoptic and local-scale meteorological phenomena also complicate conditions associated with  
119 wake vortices developing near Sumatra. Convectively coupled equatorial waves, such as equatorial  
120 Rossby or Kelvin waves, have been shown to assist tropical cyclogenesis (Bessafi and Wheeler  
121 2006; Frank and Roundy 2006; Roundy 2008; Schreck and Molinari 2009, 2011; MacRitchie  
122 and Roundy 2012; Schreck 2015). In addition, there is frequently a pronounced diurnal cycle of  
123 convection over and in proximity to Sumatra (e. g., Mori et al. 2004; Qian 2008; Wu et al. 2009).

124 This diurnal cycle may have a further influence on circulations that develop locally around the  
125 island including their shedding and movement away from the barrier.

### 126 *c. Goals of the study*

127 Analysis of terrain-induced vortex formation by topographic features in and around Sumatra  
128 and its possible role in TC formation over the Indian Ocean are explored using datasets from two  
129 field campaigns: the 2008-10 Year of Tropical Convection (YOTC) and the October-March 2011-  
130 12 Dynamics of the MJO (DYNAMO) experiment. Although the analysis period is limited to 2.5  
131 years, data from these campaigns were selected because of their high resolution (0.25 degree grid),  
132 their widespread use for studying tropical convection, and in the case of DYNAMO, the assimila-  
133 tion of field campaign data over the Indian Ocean into the analyses. Despite the high resolution,  
134 the actual processes by which the incipient circulations induced by terrain are transformed into  
135 TCs, i.e., TC genesis itself, are not adequately resolved by the data sets and are thus beyond the  
136 scope of this study. This work represents a preliminary investigation of this phenomenon, intended  
137 to motivate further process studies, as well as longer term climatologies of topographic effects on  
138 TC formation over the Indian Ocean.

## 139 **2. Data and Methods**

### 140 *a. Data*

141 The data for this study are from the YOTC and DYNAMO campaigns. YOTC was a “virtual”  
142 field experiment, conducted between May 2008 and April 2010, with a focus on gathering and  
143 assimilating existing sources of data, such as those from satellite observations or buoys, to better  
144 understand and simulate many tropical phenomena (Moncrieff et al. 2012). There were six active  
145 MJO events noted during YOTC, which passed by Sumatra in June and September 2008; February,

146 April, and November 2009; and April 2010 (Waliser et al. 2012). The active phases of the April  
147 2009 and later MJO occurrences featured stronger convection, and remained intact and propagated  
148 farther east than did the other YOTC MJO events (Waliser et al. 2012).

149 The DYNAMO campaign involved in-situ measurements by radiosonde, ship, and aircraft-based  
150 instruments in the Indian Ocean basin, where the MJO typically initiates (Yoneyama et al. 2013;  
151 Johnson and Ciesielski 2013). The special observing period (SOP), which featured the greatest  
152 spatial and temporal density of observations, ran from 1 October to 15 December 2011, followed  
153 by a period of less-intense observations through the end of March 2012. There were two MJO  
154 events during the DYNAMO SOP, in October and November. The November MJO event was noted  
155 for its strong convection, two westerly wind bursts, and the interaction of Kelvin waves, equatorial  
156 Rossby waves, and nascent TC development over the northern Indian Ocean (Gottschalck et al.  
157 2013; Kerns and Chen 2014; Judt and Chen 2014; Oh et al. 2015).

158 A reanalysis dataset for YOTC (1 May 2008 to 30 April 2010) and the operational analysis (OA)  
159 dataset for DYNAMO (1 October 2011 to 31 March 2012) were produced by the European Centre  
160 for Medium-range Weather Forecasting (ECMWF). These datasets were created by a component  
161 of ECMWF's global model running at an enhanced resolution with observations during YOTC  
162 and DYNAMO assimilated into the model (Moncrieff et al. 2012; Johnson and Ciesielski 2013).  
163 For both datasets, the spatial resolution is  $0.25^\circ$ , with 18 pressure levels available between the  
164 surface and 50 hPa, and the temporal resolution is 6-hourly. It should be kept in mind that the  
165 YOTC period is two years, whereas the DYNAMO period is six months, so comparison of annual  
166 distributions from the two campaigns is not possible.

167 As a proxy for convective activity, outgoing longwave radiation (OLR) data at  $1^\circ$  resolution from  
168 the National Oceanic and Atmospheric Administration (NOAA) Earth System Research Labora-  
169 tory (ESRL), Boulder, Colorado ([www.esrl.noaa.gov/psd](http://www.esrl.noaa.gov/psd); Lee 2014) have been utilized.

170 Tropical cyclone track, intensity, and naming designations were obtained from best track data  
171 from the Joint Typhoon Warning Center (JTWC) as well as from NOAA's International Best Track  
172 Archive for Climate Science (IBTrACS) website ([www.ncdc.noaa.gov/ibtracs](http://www.ncdc.noaa.gov/ibtracs)).

173 *b. Methods and definition of analysis regions*

174 In order to determine the origin of terrain-induced circulations that ultimately led to TC genesis,  
175 a procedure is needed to identify and track the circulation features. While most of the prominent  
176 circulations can be identified and tracked subjectively, the limitations of such an approach as well  
177 as the large number of cases during the 2.5 years of study of both non-shed and shed circulations,  
178 demands that an objective procedure be used. Hence, the identification and tracking of vortices  
179 was carried out using the objective feature tracking code of Hodges (1995, 1999). While the  
180 cyclonic circulation features were commonly associated with negative height anomalies, as shown  
181 by Duvel (2015) for the southern Indian Ocean, many of the circulations tracked very close to  
182 or even crossed the equator, which has led to the use of relative vorticity for tracking. Relative  
183 vorticity fields at 6-h and  $0.25^\circ$  horizontal resolution from the YOTC analyses (May 2008 to April  
184 2010) and ECMWF OA (October 2011 to March 2012) were vertically averaged over the 925-850  
185 hPa layer, then smoothed to retain spatial scales greater than 450 km. Sensitivity test showed that  
186 changes to the smoothing cutoff length had no notable impact on the identification of vortices.  
187 The vertical averaging of vorticity was used to improve the temporal coherency of features when  
188 a vorticity maximum shifts between different model levels (Serra et al. 2010). Cyclonic vorticity  
189 features were tracked if their peak amplitude was greater than  $1.0 \times 10^{-5} \text{ s}^{-1}$  and they persisted  
190 for longer than 2 days. This threshold is larger than that used by Serra et al. (2010) for African  
191 Easterly Waves, but sensitivity tests show that this value effectively captures significant vortex  
192 features that have the potential to contribute to TC genesis.

193 To focus on vortex wakes that transitioned into Indian Ocean tropical storms, we restrict our  
194 analyses only to cases in which the vortex shed westward over the Indian Ocean. To differentiate  
195 between westward-shedding and non-shed vortices, shed vortices are defined as those with (1) a  
196 final location over the Indian Ocean that is  $> 500$  km from Sumatra, and either (2) final minus  
197 initial distance from Sumatra is  $> 250$  km, or (3) their average speed away from Sumatra is  $> 0.5$   
198  $\text{m s}^{-1}$ . Condition (1) ensures that the shed vortex at the end of its track is some critical distance  
199 from Sumatra and (2) or (3) ensure that it is moving away from this land mass.

200 Application of the tracking code to the 2.5 years of data yields information on both genesis lo-  
201 cations and tracks of the cyclonic vortices. Genesis locations are shown in Fig. 2, separately for  
202 the boreal cold (November-April) and warm (May-October) seasons. During the boreal winter  
203 monsoon (Fig. 2a), northeasterly flow across the Malay Peninsula and the northern tip of Suma-  
204 tra produces a high frequency of lee vortices just downstream of these topographic features. To  
205 quantify relationships between the flow and downstream circulations in these regions (to be shown  
206 later), two analysis boxes are defined in Fig. 2a: SN (Sumatra north) and MP (Malay Peninsula).  
207 There are also genesis maxima across the northern parts of Sri Lanka and the Western Ghats, as  
208 well as a broad area of genesis sites (unrelated to topography) in the southern ITCZ (Duvel 2015).

209 During the boreal summer monsoon, southeasterly flow across west Java and the southern tip of  
210 Sumatra leads to two genesis maxima in those locations (Fig. 2b). Regions SS (Sumatra south)  
211 and JV (Java), defined for later analyses, encompass these maxima. Similar to SN and MP, these  
212 regions are downstream of the relevant topographic features, indicating the majority are wake  
213 vortices. There are also maxima at the southern tip of India and southeast of Sri Lanka, as well as  
214 through a gap in the Bukit Barisan mountain range on Sumatra. However, these maxima, as well  
215 as those over India and Sri Lanka in the cold season, likely do not contribute to TC genesis, so  
216 they will not be considered in our analysis.

217 To delineate easterly and westerly flow regimes, which determine where terrain-induced vortices  
218 will form and move in relation to the topography, two computation line segments are identified in  
219 Fig. 1 (3-7°N, 100°E and 3-7°S, 105°E). Averages of the zonal wind along these lines (defined as  
220  $U_N$  and  $U_S$ , respectively) are considered representative of the flow in the analysis boxes adjacent  
221 to them. To determine the likelihood of flow blocking or splitting by the topographic features in  
222 the regions, Froude numbers were evaluated in proximity to these line segments using zonal wind  
223 speed and Brunt-Väisälä frequency averaged over the 950-850 hPa layer and assuming average  
224 terrain heights of 1 and 0.5 km in the north and south, respectively.

225 To identify convectively coupled equatorial waves and their relationship to the wake vortices  
226 and TC genesis, OLR anomalies were calculated from the NOAA OLR data, then filtered for  
227 different wave mode characteristics – period, wavenumber, and equivalent depth (Wheeler and  
228 Kiladis 1999) – which identify Kelvin, equatorial Rossby, MJO-type, or mixed-Rossby gravity  
229 waves (code provided by K. Straub, 2014, personal communication).

### 230 **3. Results**

#### 231 *a. Vortex statistics and tracks*

232 Terrain-induced vortices that moved westward out over the Indian Ocean and had the potential  
233 to contribute to TC genesis originated in the four analysis boxes shown in Fig. 2. Therefore, these  
234 regions are identified as the focal areas for subsequent analyses. Statistics on shed and non-shed  
235 vortices from these four regions are presented in Table 1. A total of 309 cyclonic vortices were  
236 detected in the four regions during the 2.5 years of data, 103 (33%) of which were shed, i.e., moved  
237 downstream away from their point of origination. The vast majority (90%) of the shed circulations  
238 from Sumatra north (SN) and the Malay Peninsula (MP) occurred during easterly flow, hence were

239 lee or wake vortices that detached from the terrain features. A similar high percentage (95%) of  
240 shed vortices occurred along west Java (JV) in easterly flow. The frequency for Sumatra south  
241 (SS) during easterly flow (72%) was somewhat less, indicating there were a fair number of cases  
242 with westerly flow impinging on Sumatra contributing to cyclonic circulations off the southern tip  
243 of the island. Flow conditions associated with shedding in all regions will be shown in the next  
244 subsection.

245 Also indicated in Table 1, there were 13 terrain-induced vortices that subsequently developed  
246 into named TCs: five from SN, six from SS, and two from JV. In other words, 13% of the 103  
247 shed vortices eventually became TCs during the 2.5 years of study. Tracks and other information  
248 pertaining to these events will be shown later; however, a summary of these 13 events and their  
249 relationship to the total named tropical cyclone counts in the Indian Ocean basin<sup>1</sup> for the various  
250 YOTC and DYNAMO time periods is shown in Table 2. The five TCs over the northern IO  
251 originating from terrain-induced circulations represent 31% of the total (16) TCs in the northern  
252 hemisphere during the 2.5-year period, whereas the eight TCs similarly identified for the southern  
253 IO represent 23% of the total (35) for that region. *Notably, for the entire IO basin, the 13 TCs*  
254 *originating from shed vortices represent 25% of the total (51) TCs occurring in the Indian Ocean*  
255 *basin during the period of study, highlighting the important role of topography in TC genesis in*  
256 *this region.* Moreover, these percentages likely represent a lower bound to such events since they  
257 include only cases in which the tracking program provided conclusive evidence of a wake to TC  
258 transition. Other cases may not have been captured due to limitations in the reanalysis datasets and  
259 the limitations imposed by the various tracking procedure settings (e.g., a lower vorticity amplitude  
260 threshold may have yielded longer, more continuous tracks). Finally, Table 2 also includes average

---

<sup>1</sup>The Indian Ocean basin is defined here as that portion of the Indian Ocean extending from Africa to 105°E. Tropical cyclones that formed east of 105° and moved into the IO are excluded from the tabulations.

261 TC frequencies (values in parentheses) based on a 30-yr (1985-2014) climatology of TC formation  
262 in the IO using JTWC best track and storm report data. It can be seen that the TC frequencies for  
263 the different time periods for this longer-term climatology are comparable to those for the 2.5 years  
264 of YOTC and DYNAMO, indicating that the more limited period in our study was not abnormal  
265 in terms of TC activity.

266 The monthly distributions of the shed and non-shed vortices, as well as TCs originating from  
267 terrain-induced circulations, for regions SN and MP are shown in Fig. 3. Values are shown in  
268 counts per year to take into account the fact that the data records for YOTC (two years) and  
269 DYNAMO (six months) are different. From Fig. 3 it is seen that cyclonic vortices generated by  
270 the topographic features in SN and MP occur predominantly during the boreal winter monsoon,  
271 when low-level easterly flow prevails over the region (Figs. 2a and 3c). Shedding of vortices is  
272 more common from SN than MP (Table 1), and only SN-shed vortices (five cases in October and  
273 November, representing 12% of the shed events) led to TC genesis during the 2.5 years of study.

274 Cyclonic vortices from regions SS and JV are distributed somewhat more broadly throughout the  
275 annual cycle (Fig. 4), although the majority occurred during the austral winter and spring seasons.  
276 On average, the flow across these terrain features during this period had an easterly component  
277 (Figs. 2b and 4c). However, unlike the northern Sumatra region, those terrain-induced cyclonic  
278 vortices that led to TC genesis occurred under conditions of both mean easterly and westerly flow.  
279 With respect to timing, most TC cases (5 out of 8) in the southern Indian Ocean occurred during  
280 the boreal winter monsoon, as was the case in region SN.

281 To further emphasize the importance of the topography surrounding the Indian Ocean basin for  
282 initiating cyclonic circulations, a map of all vortex tracks originating between 10°N and 10°S  
283 in this region during the 2.5 years of data is shown in Fig. 5a. The role of significant terrain  
284 features – Sumatra, the Malay Peninsula, west Java, southern India, and Sri Lanka – for generating

285 cyclonic circulations is clearly evident. Many of the circulations produced by SN and MP move  
286 due westward, whereas those from SS and JV are frequently swept northwestward off the southern  
287 coast of Sumatra by the southeasterly flow (Fig. 2b). Tracks emanating from Sri Lanka and the  
288 south tip of India occur predominantly during the fully developed winter and summer monsoons  
289 and likely do not contribute to TC genesis due to stronger vertical shear during these periods.

290 The tracks of the cyclonic circulations emanating from the four analysis boxes are shown in Fig.  
291 5b. Most tracks extend westward over the Indian Ocean and, hence, potentially can contribute to  
292 TC genesis. Indeed, a number of the tracks, including some spanning most of the entire Indian  
293 Ocean, eventually became named TCs, as will be shown later.

294 As mentioned earlier, shedding of wake vortices may be a result of boundary layer separation,  
295 perturbations in the flow, or instability in the wake (Etling 1989; Schär and Smith 1993b). Com-  
296 parison of the mean lower-tropospheric flow for shed and non-shed vortices (easterly flow cases  
297 only) for region SN (Fig. 6) reveals rather subtle flow differences across the northern tip of Suma-  
298 tra. Specifically, shed events have a slightly stronger easterly flow to the north of the island (up  
299 to  $2 \text{ m s}^{-1}$  at 700 hPa), perhaps aiding the shedding process. Similar differences are noted for  
300 shed vs. non-shed easterly flow cases for region SS (not shown). Furthermore, additional analyses  
301 of the SN cases (also not shown) indicates that for shed cases, easterly flow in the vicinity of SN  
302 increases and peaks one to two days following the initiation date of the wake vortex, whereas for  
303 non-shed cases, easterly flow diminishes following wake vortex initiation.

304 The mean flow for shed cases for region SS for both easterly and westerly flow is shown in Fig.  
305 7. Cyclonic vortex generation over the eastern Indian Ocean south of the equator in easterly flow  
306 (Fig. 7a) is in part created by southeasterly flow against the mountain barrier along the southern  
307 part of the island. However, in addition, blocking of westerly flow along and just to the north of  
308 the equator by the island is seen to partially contribute to the cyclonic circulation in this region.

309 This effect is particularly noticeable for westerly flow in region SS (Fig. 7b), where upstream  
310 blocking and splitting of equatorial westerly flow is seen to contribute to cyclonic circulations in  
311 both hemispheres. However, the flow pattern for this situation is also suggestive of a pair of Rossby  
312 gyres, which would be accompanied by equatorial westerlies impinging on Sumatra. Such a case  
313 was studied by Ridout and Flatau (2011), where the Rossby gyres near Sumatra were associated  
314 with a convectively coupled Kelvin wave. Nevertheless, blocking of equatorial westerlies by the  
315 topography of Sumatra could serve to enhance the circulations in the Rossby gyres, representing  
316 a superposition of effects contributing to vortex initiation.

#### 317 *b. Vorticity production by topography*

318 Topographically generated vorticity streamers, similar to “PV banners” investigated during the  
319 Mesoscale Alpine Programme (Aebischer and Schär 1998), are seen to be commonplace throughout  
320 the Asian-Australian monsoon region (Fig. 8). Streamlines and relative vorticity for the six-month  
321 DYNAMO period are shown in Fig. 8a for easterly 925-850 hPa flow across northern Sumatra ( $U_N$ )  
322 having a magnitude exceeding  $5 \text{ m s}^{-1}$ . A positive vorticity maximum is observed at the northern  
323 tip of Sumatra, consistent with the observation of frequent vortex generation just downstream (Fig.  
324 2a). A streamer of vorticity extends due westward into the Indian Ocean, suggestive of frequent  
325 shedding of these vortices. The average Froude number (Fr) in the 950-850 hPa layer under the  
326 easterly flow regimes was  $\sim 0.3$ , supporting flow blocking and splitting by Sumatra’s mountains  
327 (Smith 1989; Smolarkiewicz and Rotunno 1989). Positive vorticity is also observed downstream of  
328 the northern periphery of other islands in the maritime continent such as Borneo, the island of Sri  
329 Lanka, and significant topographic features elsewhere in the region. Negative geopotential height  
330 anomalies were observed in the center of these cyclonic vortices (not shown here, but illustrated  
331 later), consistent with the findings of Schär and Smith (1993b).

332 For the flow conditions used to produce Fig. 8a, cyclonic vorticity can also be seen downstream  
333 of the southern tip of Sumatra, with a closed circulation offshore extending into a broad expanse  
334 of negative vorticity across most of the Indian Ocean between the equator and  $10^{\circ}\text{S}$ .<sup>2</sup> This broad  
335 trough region reflects the existence of the southern Indian Ocean ITCZ. Froude numbers associated  
336 with easterly flow for the southern regions were  $\sim 0.7$ , suggesting a slightly weaker blocking effect  
337 by the southern portion of the island, principally due to the lower average topography there (Fig.  
338 1).

339 During low-level westerly flow across the northern tip of Sumatra, anticyclonic relative vorticity  
340 was observed along Sumatra's northern tip (Fig. 8b), as well as to the lee of the Malay Peninsula  
341 and at the north coast of Borneo. During this period, the southern ITCZ (indicated by cyclonic or  
342 negative vorticity) was still present, though shifted slightly equatorward.

343 To better quantify the relationship between zonal wind and the circulation downstream of Sumatra,  
344 relative vorticity averaged within each of the analysis regions was regressed onto zonal winds  
345  $U_N$  or  $U_S$  (as appropriate for their respective hemispheres) at different levels in the lower tropo-  
346 sphere. Peak correlations were found to occur in the height range from 925 to 850 hPa level in  
347 the north and 950 to 1000 hPa in the south, with correlations dropping off at higher levels (Fig. 9).  
348 This behavior is consistent with expected flow blocking for topography with an average height of  
349 1-2 km in the northern Sumatra region and somewhat lower in the south. The weaker correlations  
350 near the surface in regions SN, MP, and SS are likely related to weaker surface flow in those areas  
351 due to blocking by topography, while the differing correlation patterns at higher levels are related  
352 to different mean flow patterns in the north vs. south regions. Considering these findings, a level  
353 of 900 hPa is chosen to illustrate correlations between zonal wind and relative vorticity for all four

---

<sup>2</sup>The flow pattern illustrated in Fig. 8a closely resembles that depicted by Kuettner (1989) as an archetype of the circulation associated with twin cyclone development in the eastern Indian Ocean, leading him to propose Sumatra as a potential generator of incipient TC disturbances.

354 regions (Fig. 10). For the entire 2.5 year period, cyclonic (positive) vorticity in regions SN and  
355 MP (Fig. 10, top panels) was negatively correlated to the zonal wind (all correlations significant  
356 at the 99% level). In other words, the stronger the oncoming flow, the stronger the vorticity in the  
357 analysis regions.

358 In regions SS and JV (Fig. 10, bottom panels), correlations between 900-hPa zonal wind and  
359 relative vorticity were poorer than those for the northern regions. This is not unexpected since  
360 the average topography is lower in the south (Fig. 1). In addition, the mean vorticity is nearly  
361 always cyclonic off the southwest coast of Sumatra due to the relatively persistent ITCZ, which  
362 migrates north and south throughout the year (Fig. 2). The persistence of cyclonic vorticity near  
363 southern Sumatra regardless of flow direction is evident in Fig. 10 (bottom panels) where most of  
364 the relative vorticity values are negative for easterly flow cases and the majority are also negative  
365 for westerly flow cases.

### 366 *c. Vortex shedding as a precursor to tropical cyclone development*

367 Once formed, terrain-produced vortices often shed and move downstream. Potential vorticity  
368 anomalies within the circulations can persist as they move downstream, unless acted upon by  
369 dissipative processes. While it would be instructive to elucidate the mechanisms for shedding in  
370 our study region, data adequate to do so (e.g., field campaign data in proximity to Sumatra) are  
371 not available.

372 The formation and downstream movement of cyclonic vortices for the latitudes of both northern  
373 and southern Sumatra are shown for the YOTC and DYNAMO years in wind-vorticity Hovmöller  
374 diagrams shown in Figs. 11-13. All of the TCs traced back to cyclonic vortices generated by  
375 Sumatra's topography in the *northern* Indian Ocean during the YOTC and DYNAMO periods  
376 occurred during the months of OND (Table 3). During the OND periods for all three years, positive

377 vorticity maxima at 850 hPa frequently occur near 95°E in region SN just west of Sumatra's  
378 northern tip (Figs. 11a, 12a, and 13a). Similarly, in Figs. 11-13, frequent vorticity maxima can  
379 also be seen at the longitudes of the other regions: MP (~100-102°E), SS (~100°E), and JV  
380 (~105°E). Farther east, other positive/negative vorticity anomalies are evident and associated with  
381 terrain features in the maritime continent (Fig. 8a).

382 The common occurrence of positive vorticity maxima at the longitude of Sumatra's northern  
383 tip during easterly flow is evidence of persistent lee vortex formation. On occasion, however, the  
384 positive vorticity anomalies detach from Sumatra and move westward. Three instances of such  
385 events directly associated with TC development in 2008 are depicted in Fig. 11a: TC 03A in  
386 October, Nisha in November, and TC 07B in December.<sup>3</sup>

387 A similar pattern of cyclonic (negative) vorticity maxima near 95°E just west of Sumatra's south-  
388 ern tip is seen in Fig. 11b (fields are at 925 hPa due to lower topography there) although its asso-  
389 ciation solely with easterly flow is less obvious than in northern Sumatra. One westward-moving  
390 vorticity streamer in October was a precursor to TC Asma, the southern Indian Ocean counterpart  
391 to TC 03A.

392 During the 2009 OND YOTC period, vorticity maxima once again occurred near Sumatra's  
393 northern tip associated with lee vortex formation, and several instances of shedding vortices were  
394 evident in November (Fig. 12a). However, TC Ward was the only northern Indian Ocean storm  
395 during the OND 2009 period to develop from a lee vortex. Over the southern Indian Ocean, TCs  
396 Cleo and David (Fig. 12b) formed around the time of TC Ward, collectively constituting cross-  
397 equatorial "triplets" in December 2009. Cleo and David both reached tropical storm wind speeds  
398 following the end of vorticity streamers depicted within the southern Sumatra latitude band (Fig.

---

<sup>3</sup>In the case of TC 03A and several others shown later, the location of the storm symbol is displaced outside the vorticity streamer in the time-longitude diagrams since the official naming of the TC occurred when the center was outside the 3-7° latitude band.

399 12b), although it is difficult to identify each storm with a particular shed vortex in this depiction  
400 since the wake vortices moved out of the 3-7°S latitude band before intensifying. The continuity of  
401 these circulations will become more apparent in the discussion of individual cases in the following  
402 subsection.

403 During the DYNAMO year, the three instances where wake vortices propagated westward and  
404 eventually became tropical cyclones – TC 05A in the northern hemisphere and TCs Alenga and  
405 Benilde in the southern hemisphere – are indicated in Fig. 13. There are also a number of shed  
406 wake vortices (vorticity streamers) in both hemispheres that did not develop into tropical cyclones.  
407 However, two of the TCs that developed, 05A and Alenga, moved into a favorable environment for  
408 TC genesis provided by the developing MJO over the central Indian Ocean (Yoneyama et al. 2013;  
409 Gottschalck et al. 2013). Prominent vorticity maxima immediately to the west of Sumatra's tips  
410 regularly occurred during periods of low-level easterly flow at 850 hPa in both the northern (Fig.  
411 13a) and southern (Fig. 13b) hemispheres, with westward movement of streamers in a number of  
412 instances.

413 In summary, results for the YOTC and DYNAMO years indicate that when easterly wind im-  
414 pinged upon Sumatra, multiple wake vortices were observed to form and propagate away in suc-  
415 cession, e.g., in November 2009 (Fig. 12a), and in the easterly wind periods that preceded the  
416 late October and November 2011 MJO events (Fig. 13a). However, in some instances, as will be  
417 evident in the cases presented later, augmentation of cyclonic vorticity appeared to occur when  
418 *westerly* equatorial wind impacted central Sumatra as well. In these situations the high terrain on  
419 the western side of Sumatra blocked low-level equatorial westerly flow, diverting it to the north  
420 and south, so that when combined with easterly flow across Sumatra's tips, cyclonic vorticity was  
421 enhanced in those locations.

422 The southern Indian Ocean near Sumatra demonstrated a weak secondary maximum in shed vor-  
423 tex occurrence between March and May (Figs. 4a,b), another period of climatologically frequent  
424 tropical cyclogenesis in the Indian Ocean. Two TCs originating from terrain-induced vortices  
425 from region SS occurred during this period (in March), while another occurred in January (Fig.  
426 4b). The remaining southern hemisphere TCs traced back to terrain-induced vortices (five of them)  
427 occurred between October and December.

428 In total, ten TCs during YOTC, and three during DYNAMO, were determined to have developed  
429 from cyclonic vortices that formed downstream of Sumatra and adjacent land masses. Three TCs,  
430 Gael (2009) during YOTC and 05A and Alenga (2011) during DYNAMO, formed in the easterly  
431 flow regimes preceding the active phase of MJO events. The tracks of all of the wake vortices that  
432 eventually developed into tropical cyclones during the two years of YOTC and the DYNAMO SOP  
433 are plotted in Fig. 14. The pre-TC periods of the tracked vortices are marked by thin lines, the  
434 named-storm periods by thick lines. Several of the vortices remained coherent and traversed much  
435 of the Indian Ocean basin before they intensified and were named by the responsible agencies,  
436 while others intensified closer to Sumatra. Three sets of cross-equatorial, companion tropical  
437 cyclones that originated from wake vortices during the analyzed time periods were TCs 03A and  
438 Asma in October 2008; TCs Cleo, Ward, and David in December 2009; and TCs 05A and Alenga  
439 in late November and early December 2011.

440 The 13 TCs identified to have originated from terrain-induced circulations during YOTC and  
441 DYNAMO are listed in Table 3. The length of time from vortex genesis to naming of the storms  
442 by operational centers ranged from 5 to 20 days, with an average duration of 10.1 days, indicating  
443 a long gestation period for many of the disturbances prior to TC genesis. Comparing results from  
444 Tables 1 and 2, 9% (18%) of the vortices identified using the vorticity threshold of  $1.0 \times 10^{-5} \text{ s}^{-1}$   
445 that shed from the northern (southern) regions of Sumatra, or 13% of the total, eventually became

446 named TCs. As mentioned earlier, these TCs comprised nearly one-quarter of all TCs occurring  
447 in the Indian Ocean basin during the period of study.

#### 448 *d. Selected case studies*

449 In this section, tropical cyclones Cleo, Ward, and David in 2009 and 05A in 2011 have been  
450 selected to illustrate cyclonic vortex development, associated geopotential height falls, and sub-  
451 sequent transformation into TCs. Detailed mechanisms involved in their transformations, i.e., the  
452 process of TC genesis, cannot be fully determined from the available data, so this aspect of their  
453 life cycles is beyond the scope of this study. The full tracks of the TCs, beginning as wake vortices  
454 near Sumatra, are shown in Fig. 14.

455 TCs Cleo, Ward, and David can be considered “triplet” storms in December 2009. The wake  
456 vortex precursor to TC Cleo in the southern hemisphere appeared to be assisted by blocking of  
457 westerly equatorial flow by central Sumatra in late November 2009. The vortex is near 100°E on 2  
458 December with lower geopotential heights already at its center (Fig. 15a). Cleo eventually became  
459 a named storm on 7 December. At the same time, a lee vortex appeared on the north end of the  
460 island, which would eventually become TC Ward on 11 December (Figs. 14 and 15b-c). Low-level  
461 flow near southern Sumatra shifted to easterly on 3 December and along with blocked equatorial  
462 westerlies resulted in a second cyclonic wake vortex in the southern Indian Ocean, which would  
463 later move westward and intensify into TC David (Fig. 15e-f), which was named on 13 December.  
464 In the cases of all three storms, no apparent upstream cyclonic vorticity maxima were present prior  
465 to the wake vortex initiation (Fig. 12). Strong ( $u > 7 \text{ m s}^{-1}$ ) low-level equatorial westerlies were  
466 present over the eastern Indian Ocean through the lifecycle of these burgeoning wake vortices,  
467 which, together with low-level trade easterlies farther poleward, constituted cyclonic shear in both  
468 hemispheres. At their peak intensities, TCs Cleo and Ward had estimated winds up to 115 and

469 45 kt, respectively. TC David reached the middle of the Indian Ocean before intensifying into a  
470 tropical storm with a maximum wind speed of 55 kt. Its remnants dumped heavy rain on Mauritius  
471 and Reunion, causing flooding and damage (La Sentinelle 2009). There was not an MJO event  
472 prior to TCs Cleo, Ward, and David, to create environmental conditions that may have enhanced  
473 the potential for TC genesis, as in the 2011 (DYNAMO) cases of TC 05A and Alenga, which will  
474 be discussed next.

475 In late-November 2011, the wake vortex that would later become TC 05A initiated off the north  
476 tip of Sumatra as easterly flow impinged upon the island (Fig. 16a). These easterlies were as-  
477 sociated with the pre-onset phase of the approaching November 2011 MJO convective envelope  
478 (Johnson and Ciesielski 2013). The vortex moved slowly westward over the next four days (Fig.  
479 16c-f), but was not officially designated TC 05A until 26 November when it was west of Sri Lanka  
480 and had encountered the moist MJO convective envelope. Though its maximum wind speed was  
481 only 35 kt, it caused damage and deaths in Sri Lanka (Agence France-Presse 2011). The wake  
482 vortex that would become TC Alenga formed ten days after the TC 05A vortex and therefore is  
483 not depicted in Fig. 16, though it too interacted with the MJO convective envelope (in a way likely  
484 similar to that described by Duvel 2015) to assist in its development, namely, by encountering  
485 enhanced north-south shear of the low-level zonal flow.

486 The development of TC 05A was also influenced by convectively coupled equatorial waves,  
487 which occurred in association with the late November 2011 active MJO event (Gottschalck et al.  
488 2013; Oh et al. 2015). A convectively coupled equatorial Rossby (ER) wave moved westward  
489 and passed over the vorticity streamer that represents the wake vortex precursor to TC 05A in late  
490 November (Fig. 17a). The initiation of the vorticity streamer around 22 November was nearly  
491 coincident with the arrival of the ER wave at the longitude of Sumatra. However, investigation of  
492 all the other cases with respect to the passage of equatorial waves (equatorial Rossby and mixed-

493 Rossby gravity) did not show any consistent or systematic pattern of vortex shedding in association  
494 with the waves (not shown). In addition, a Kelvin wave convective envelope, which featured strong  
495 OLR anomalies, propagated eastward over the same region in late November 2011 (Fig. 17b). Its  
496 encounter with the wake vortex on 25 November led to a pronounced strengthening of the vorticity  
497 at that time. Strong westerly wind bursts, apparent in Figs. 16e and f, associated with the Kelvin  
498 waves likely served to enhance the vortex's low-level cyclonic circulation. Gottschalck et al.  
499 (2013) and Oh et al. (2015) describe the combined influence of Kelvin, equatorial Rossby, and  
500 mixed-Rossby waves on the flow in the region of the developing TC 05A during this period.

#### 501 **4. Summary and conclusions**

502 This study explores the potential role of the island of Sumatra and adjacent topographic features  
503 in creating terrain-induced circulations over the Indian Ocean that later develop into tropical cy-  
504 clones (TCs). Sumatra, as well as the Malay Peninsula and Java, have mountainous terrain that  
505 partially blocks low-level flow under typical environmental stratification. For easterly low-level  
506 flow, these terrain features often produce lee vortices, some of which subsequently shed and move  
507 westward from the northern and southern tips of Sumatra and thence downstream over the Indian  
508 Ocean. Since Sumatra straddles the equator, extending in a northwest-to-southeast direction from  
509 approximately 6°N to 6°S, the lee vortices generated at the two ends, while counter-rotating, are  
510 both cyclonic. This unique situation is not found elsewhere in the tropics. The generation of TCs  
511 by Sumatra wake vortices was first proposed many years ago by Kuettner and Soules (1967) and  
512 Kuettner (1989), although little attention has been given to it since.

513 To investigate the role of topographically induced vortices in TC formation over the IO, data  
514 from the 2008-10 Year of Tropical Convection (YOTC) and 2011-12 Dynamics of the MJO (DY-  
515 NAMO) campaigns are used. ECMWF quarter degree reanalysis and operational datasets from

516 these campaigns have provided sufficient resolution to detect and track the wake vortices that were  
517 observed to develop at the northern and southern ends of Sumatra. The identification and tracking  
518 of vortices was carried out using the objective feature tracking code of Hodges (1995, 1999). In  
519 applying this algorithm to the Indian Ocean basin, it was discovered that in addition to Sumatra,  
520 the Malay Peninsula and the mountains of west Java also contribute to cyclonic vortex develop-  
521 ment with eventual shedding of vortices into the Indian Ocean where they have the potential to  
522 influence TC genesis. Therefore, attention is focused on these two regions in addition to Sumatra  
523 itself with respect to topographic influence on the flow. The majority of the shed circulations from  
524 both northern and southern Sumatra regions occurred in easterly low-level flow, hence were lee or  
525 wake vortices. However, some instances of blocking and splitting of low-level westerly equatorial  
526 flow by the mountainous island of Sumatra contributed to cyclonic circulations *upstream* of the  
527 island.

528 Key findings of this study are as follows:

- 529 1. Sumatra and the Malay Peninsula and west Java are prolific generators of low-level topo-  
530 graphically induced circulations, contributing during YOTC and DYNAMO to 309 cyclonic  
531 circulations having an amplitude threshold of  $1.0 \times 10^{-5} \text{ s}^{-1}$  trackable over at least a two-day  
532 period. Of these, 33% were shed, i.e., moved downstream from their point of origination.
- 533 2. During the 2.5 years of the two campaigns<sup>4</sup>, 13 TCs (five in the northern hemisphere and  
534 eight in the southern hemisphere) originated from shed vortices, representing 13% of all shed  
535 events. *These 13 TCs constituted 25% of all the TCs occurring in the Indian Ocean basin*  
536 *during the period of study, indicating the important role of topography in TC genesis in the*  
537 *region.*

---

<sup>4</sup>While the YOTC and DYNAMO time span is limited to 2.5 years, a comparison of TC frequencies during these field campaigns to those of a 30-yr (1985-2014) climatology reveals that TC activity during the YOTC-DYNAMO period was quite close to normal.

538 3. For shed vortices that eventually became TCs, the average length of time from vortex genesis  
539 to the naming of the storms was 10.1 days, indicating a relatively long gestation period for  
540 these TC precursor disturbances.

541 Though terrain-induced vortices occurred throughout much of the year, the occurrence of TC  
542 genesis was in most cases (10 out of 13) confined to the October-December period due to the  
543 low environmental vertical wind shear as the monsoon transitions from boreal summer to winter.  
544 The results are consistent with those of Kuettner (1989), who found that all but one twin TC case  
545 described in his study developed between October and December.

546 In four of the cases during YOTC and DYNAMO, easterly winds preceding the onset of the  
547 MJO's active phase encountered Sumatra, producing cyclonic wake vortices that formed and  
548 moved westward, subsequently interacting with the MJO convective envelope before develop-  
549 ing into tropical storms. In the TC 05A case that occurred during DYNAMO, both the MJO and  
550 equatorial waves (equatorial Rossby, mixed-Rossby gravity, and Kelvin waves) appeared to con-  
551 tribute to the development of the TC (Gottschalck et al. 2013; Judt and Chen 2014; Oh et al. 2015),  
552 although these studies did not indicate the potential role of Sumatra wake vortices in providing the  
553 initial disturbance for the TC. Equatorial waves may have supported tropical cyclogenesis by pro-  
554 ducing low-level cyclonic vorticity and lowering vertical wind shear, as detailed in other studies  
555 (e. g., Frank and Roundy 2006), although the specifics of those processes have not been investi-  
556 gated here. In addition, Sumatra represents a unique situation of superposition of effects where  
557 Rossby gyres associated with convectively coupled Kelvin waves or the MJO can have their cir-  
558 culations enhanced when westerly equatorial flow is blocked upon encountering the island.

559 This study has provided further evidence for the idea first proposed by Kuettner and Soules  
560 (1967) and Kuettner (1989) that Sumatra may serve as a generator of wake vortices that subse-

561 quently develop into tropical cyclones. It has also been found, however, that the adjacent topogra-  
562 phy on the Malay Peninsula and west Java is an important contributor to terrain-induced vortices  
563 that move out over the Indian Ocean. Not all wake vortices develop into TCs, of course, since  
564 favorable environmental conditions are required for TC genesis to occur. The MJO and equatorial  
565 waves may provide those favorable conditions, though they are not a prerequisite for TC genesis.  
566 These observational findings from the YOTC and DYNAMO campaigns motivate more extensive  
567 climatological studies of this phenomenon as well as numerical simulations to further explore the  
568 mechanisms for this unique role of topography in TC genesis over the Indian Ocean.

569 *Acknowledgments.* We are indebted to Kevin Hodges of the University of Reading for providing  
570 his tracking code for our study and his assistance in setting it up for our application. We also thank  
571 Kathy Straub for providing the code for identifying convectively coupled equatorial wave modes.  
572 Comments and suggestions of two anonymous reviewers have led to significant improvements in  
573 the manuscript. The DYNAMO operational and YOTC reanalysis data sets were made available  
574 by the European Centre for Medium-Range Weather Forecasts. This work has been supported by  
575 National Science Foundation grants AGS-1059899, AGS-1138353 and AGS-1360237, a one-year  
576 American Meteorological Society Fellowship awarded to Caitlin Fine, and the United States Navy.

## 577 **References**

578 Aebischer, U., and C. Schär, 1998: Low-level potential vorticity and cyclogenesis to the lee of the  
579 Alps. *J. Atmos. Sci.*, **55**, 186–207.

580 Agence France-Presse, 2011: Sri Lanka storm kills 19, damages 5700 homes. [Available online at  
581 <http://www.webcitation.org/63Vnhm01u>].

582 Bessafi, M., and M. C. Wheeler, 2006: Modulation of South Indian Ocean tropical cyclones by  
583 the Madden-Julian Oscillation and convectively coupled equatorial waves. *Mon. Wea. Rev.*, **134**,  
584 638–656.

585 Duvel, J. P., 2015: Initiation and intensification of tropical depressions over the southern Indian  
586 Ocean: Influence of the MJO. *Mon. Wea. Rev.*, **143**, 2170–2191.

587 Epifanio, C. C., 2003: Lee vortices. *Encyclopedia of Atmospheric Sciences*, J. R. Holton, J. Pyle,  
588 and J. A. Curry, Eds., Elsevier Science Ltd., 1150–1160.

589 Epifanio, C. C., and D. R. Durran, 2002: Lee-vortex formation in free-slip stratified flow over  
590 ridges. Part I: Comparison of inviscid theory and fully nonlinear viscous simulations. *J. Atmos.*  
591 *Sci.*, **59**, 1153–1165.

592 Etling, D., 1989: On atmospheric vortex streets in the wake of large islands. *Meteorology and*  
593 *Atmospheric Physics*, **41**, 157–164.

594 Farfán, L. M., and J. A. Zehnder, 1997: Orographic influence on the synoptic-scale circulations  
595 associated with the genesis of Hurricane Guillermo (1991). *Mon. Wea. Rev.*, **125**, 2683–2698.

596 Frank, W. M., and P. E. Roundy, 2006: The role of tropical waves in tropical cyclogenesis. *Mon.*  
597 *Wea. Rev.*, **134**, 2397–2417.

598 Gottschalck, J., P. E. Roundy, C. J. Schreck III, A. Vintzileos, and C. Zhang, 2013: Large-scale  
599 atmospheric and oceanic conditions during the 2011–12 DYNAMO field campaign. *Mon. Wea.*  
600 *Rev.*, **141**, 4173–4196.

601 Gray, W. M., 1968: Global view of the origin of tropical disturbances and storms. *Mon. Wea. Rev.*,  
602 **96**, 669–700.

603 Hodges, K., 1995: Feature tracking on the unit sphere. *Mon. Wea. Rev.*, **123**, 3458–3465.

604 Hodges, K., 1999: Adaptive constraints for feature tracking. *Mon. Wea. Rev.*, **127**, 1362–1373.

605 Inness, P., and J. Slingo, 2006: The interaction of the Madden-Julian Oscillation with the Maritime  
606 Continent in a GCM. *Quart. J. Roy. Meteor. Soc.*, **132**, 1645–1667.

607 Johnson, R. H., and P. E. Ciesielski, 2013: Structure and properties of Madden–Julian oscillations  
608 deduced from DYNAMO sounding arrays. *J. Atmos. Sci.*, **70**, 3157–3179.

609 Judt, F., and S. S. Chen, 2014: An explosive convective cloud system and its environmental condi-  
610 tions in MJO initiation observed during DYNAMO. *J. Geophys. Res. Atmos.*, **119**, 2781–2795.

611 Kerns, B., and S. S. Chen, 2014: Equatorial dry air intrusion and related synoptic variability in  
612 MJO initiation during DYNAMO. *Mon. Wea. Rev.*, **142**, 1326–1343.

613 Kuettner, J., 1989: Easterly flow over the cross equatorial island of Sumatra and its role in the  
614 formation of cyclone pairs over the Indian Ocean. *Wetter und Leben*, **41**, 47–55.

615 Kuettner, J., and S. Soules, 1967: Types and scales of equatorial circulations as revealed from  
616 space and their possible exploration by tropical field projects. *Proc. 5th Technical Conference  
617 on Hurricanes and Tropical Meteorology*, Caracas, Venezuela, Royal. Meteor. Soc.

618 La Sentinelle, 2009: Pluies diluviennes: les pompiers et la Special Mo-  
619 bile Force en état d’alert. [Available online at [http://www.lexpress.mu/article/  
620 pluies-diluviennes-les-pompiers-et-la-special-mobile-force-en-%C3%A9tat-d%E2%80%  
621 99alerte/](http://www.lexpress.mu/article/pluies-diluviennes-les-pompiers-et-la-special-mobile-force-en-%C3%A9tat-d%E2%80%99alerte/)].

622 Lee, H.-T., 2014: Outgoing Longwave Radiation (OLR) - Daily. NOAA’s Climate Data Record  
623 (CDR) program. Climate algorithm theoretical basis document (c-atbd), National Center for  
624 Atmospheric Research, Boulder, CO, 46 pp.

- 625 MacRitchie, K., and P. E. Roundy, 2012: Potential vorticity accumulation following atmospheric  
626 Kelvin waves in the active convective region of the MJO. *J. Atmos. Sci.*, **69**, 908–914.
- 627 Madden, R. A., and P. R. Julian, 1971: Detection of a 40-50 day oscillation in the zonal wind in  
628 the tropical Pacific. *J. Atmos. Sci.*, **28**, 702–708.
- 629 Madden, R. A., and P. R. Julian, 1972: Description of global-scale circulation cells in the tropics  
630 with a 40-50 day period. *J. Atmos. Sci.*, **29**, 1109–1123.
- 631 Moncrieff, M. W., D. E. Waliser, M. J. Miller, M. A. Shapiro, G. R. Asrar, and J. Caughey, 2012:  
632 Multiscale convective organization and the YOTC virtual global field campaign. *Bull. Amer.*  
633 *Meteor. Soc.*, **93**, 1171–1187.
- 634 Mori, S., and Coauthors, 2004: Diurnal land-sea rainfall peak migration over Sumatera Island, In-  
635 donesian maritime continent, observed by TRMM satellite and intensive rawinsonde soundings.  
636 *Mon. Wea. Rev.*, **132**, 2021–2039.
- 637 Oh, J.-H., X. Jiang, D. E. Waliser, M. W. Moncrieff, R. H. Johnson, and P. Ciesielski, 2015: A mo-  
638 mentum budget analysis of westerly wind events associated with the Madden–Julian Oscillation  
639 during DYNAMO. *J. Atmos. Sci.*, **72**, 3780–3799.
- 640 Qian, J.-H., 2008: Why precipitation is mostly concentrated over islands in the Maritime Conti-  
641 nent. *J. Atmos. Sci.*, **65**, 1428–1441.
- 642 Ridout, J., and M. Flatau, 2011: Convectively coupled Kelvin wave propagation past Suma-  
643 tra: A June case and corresponding composite analysis. *J. Geophys. Res.*, **116**, doi:10.1029/  
644 2010JD014981.
- 645 Rotunno, R., and P. K. Smolarkiewicz, 1991: Further results on lee vortices in low-Froude-number  
646 flow. *J. Atmos. Sci.*, **48**, 2204–2211.

- 647 Roundy, P. E., 2008: Analysis of convectively coupled Kelvin waves in the Indian Ocean MJO. *J.*  
648 *Atmos. Sci.*, **65**, 1342–1359.
- 649 Schär, C., and R. B. Smith, 1993a: Shallow-water flow past isolated topography. Part I: Vorticity  
650 production and wake formation. *J. Atmos. Sci.*, **50**, 1373–1400.
- 651 Schär, C., and R. B. Smith, 1993b: Shallow-water flow past isolated topography. Part II: Transition  
652 to vortex shedding. *J. Atmos. Sci.*, **50**, 1401–1412.
- 653 Schreck, C. J., 2015: Kelvin waves and tropical cyclogenesis: A global survey. *Mon. Wea. Rev.*,  
654 **143**, 3996–4011.
- 655 Schreck, C. J., and J. Molinari, 2009: A case study of an outbreak of twin tropical cyclones. *Mon.*  
656 *Wea. Rev.*, **137**, 863–875.
- 657 Schreck, C. J., and J. Molinari, 2011: Tropical cyclogenesis associated with Kelvin waves and the  
658 Madden-Julian Oscillation. *Mon. Wea. Rev.*, **139**, 2723–2734.
- 659 Serra, Y., G. Kiladis, and K. Hodges, 2010: Tracking and mean structure of easterly waves over  
660 the Intra-Americas seas. *J. Climate*, **23**, 4823–4840.
- 661 Smith, R. B., 1989: Hydrostatic flow over mountains. *Advances in Geophysics*, **31**, 1–41.
- 662 Smolarkiewicz, P. K., and R. Rotunno, 1989: Low Froude number flow past three-dimensional  
663 obstacles. Part I: Baroclinically generated lee vortices. *J. Atmos. Sci.*, **46**, 1154–1164.
- 664 Waliser, D. E., and Coauthors, 2012: The “Year” of Tropical Convection (May 2008–April 2010):  
665 Climate variability and weather highlights. *Bull. Amer. Meteor. Soc.*, **93**, 1189–1218.
- 666 Wheeler, M., and G. N. Kiladis, 1999: Convectively coupled equatorial waves: Analysis of clouds  
667 and temperature in the wavenumber-frequency domain. *J. Atmos. Sci.*, **56**, 374–399.

- 668 Wu, C.-H., and H.-H. Hsu, 2009: Topographic influence on the MJO in the Maritime Continent.  
669 *J. Climate*, **22**, 5433–5448.
- 670 Wu, P., M. Hara, J.-i. Hamada, M. D. Yamanaka, and F. Kimura, 2009: Why a large amount of rain  
671 falls over the sea in the vicinity of western Sumatra Island during nighttime. *J. Appl. Meteor.*  
672 *Climatol.*, **48**, 1345–1361.
- 673 Yoneyama, K., C. Zhang, and C. N. Long, 2013: Tracking pulses of the Madden-Julian Oscillation.  
674 *Bull. Amer. Meteor. Soc.*, **94**, 1871–1891.
- 675 Zehnder, J. A., D. M. Powell, and D. L. Ropp, 1999: The interaction of easterly waves, orography,  
676 and the intertropical convergence zone in the genesis of eastern Pacific tropical cyclones. *Mon.*  
677 *Wea. Rev.*, **127**, 1566–1585.
- 678 Zhang, C., 2005: Madden-Julian Oscillation. *Rev. Geophys.*, **89**, RG2003, doi:10.1029/  
679 2004RG000158.

680 **LIST OF TABLES**

681 **Table 1.** Vortices (shed and non-shed) and tropical cyclones originating from the four  
682 analysis regions in Fig. 2, including totals for easterly ( $U_N < 0$  for SN and MP,  
683  $U_S < 0$  for SS and JV) and westerly ( $U_N > 0$  for SN and MP,  $U_S > 0$  for SS and  
684 JV) flow regimes. . . . . 33

685 **Table 2.** Yearly and summary totals of tropical cyclones (TCs) in the northern and south-  
686 ern Indian Ocean (IO) that formed to the west of  $105^\circ\text{E}$  during YOTC and DY-  
687 NAMO, including numbers and percentages of tropical cyclones originating  
688 from terrain-induced vortices. Numbers in parentheses are means from a 30-  
689 yr (1985-2014) climatology of TCs that formed in the IO basin, indicating that  
690 the TC activity during the YOTC-DYNAMO periods was close to the long-term  
691 means. . . . . 34

692 **Table 3.** The 13 terrain-induced vortices that developed into named tropical cyclones  
693 originating from three analysis regions in Fig. 2 – Sumatra North (SN), Sumatra  
694 South (SS), and Java (JV) – during YOTC and DYNAMO. . . . . 35

695 TABLE 1. Vortices (shed and non-shed) and tropical cyclones originating from the four analysis regions in  
696 Fig. 2, including totals for easterly ( $U_N < 0$  for SN and MP,  $U_S < 0$  for SS and JV) and westerly ( $U_N > 0$  for SN  
697 and MP,  $U_S > 0$  for SS and JV) flow regimes.

	GENESIS REGION				
	Sumatra	Malay	Sumatra	Java (JV)	Total
	North (SN)	Peninsula (MP)	South (SS)		
Total vortices	73	85	74	77	309
Shed vortices (total)	43	15	25	20	103
Shed vortices (easterly flow)	40	12	18	19	89
Shed vortices (westerly flow)	3	3	7	1	14
Non-shed vortices (total)	30	70	49	57	206
Non-shed vortices (easterly flow)	26	61	36	40	163
Non-shed vortices (westerly flow)	4	9	13	17	43
Tropical cyclones	5	0	6	2	13

698 TABLE 2. Yearly and summary totals of tropical cyclones (TCs) in the northern and southern Indian Ocean  
699 (IO) that formed to the west of 105°E during YOTC and DYNAMO, including numbers and percentages of  
700 tropical cyclones originating from terrain-induced vortices. Numbers in parentheses are means from a 30-yr  
701 (1985-2014) climatology of TCs that formed in the IO basin, indicating that the TC activity during the YOTC-  
702 DYNAMO periods was close to the long-term means.

Period	Northern IO	Southern IO	TOTAL
YOTC			
2008 (May – Dec)	6 (4.8)	4 (4.3)	10 (9.1)
2009 (Jan – Dec)	5 (5.3)	13 (12.3)	18 (17.6)
2010 (Jan – Apr)	0 (0.5)	7 (8.0)	7 (8.5)
DYNAMO			
2011 (Oct – Dec)	5 (3.1)	3 (3.1)	8 (6.2)
2012 (Jan – Mar)	0 (0.3)	8 (6.9)	8 (7.2)
TOTAL	16	35	51
Number of TCs from terrain vortices	5	8	13
Percent TCs from terrain vortices	31.3%	22.9%	25.5%

703 TABLE 3. The 13 terrain-induced vortices that developed into named tropical cyclones originating from  
704 three analysis regions in Fig. 2 – Sumatra North (SN), Sumatra South (SS), and Java (JV) – during YOTC and  
705 DYNAMO.

Storm name	Year	Vortex initiation region	First detection date	TC naming date (JTWC)	Pre-TC duration (days)
Asma	2008	JV	27 Sep	17 Oct	20
03A	2008	SN	08 Oct	21 Oct	13
Nisha	2008	SN	18 Nov	26 Nov	8
07B	2008	SN	29 Nov	04 Dec	5
Gael	2009	SS	15 Jan	03 Feb	19
Cleo	2009	SS	27 Nov	07 Dec	10
Ward	2009	SN	29 Nov	11 Dec	12
David	2009	SS	05 Dec	13 Dec	8
Imani	2010	SS	11 Mar	23 Mar	12
Robyn	2010	SS	26 Mar	02 Apr	7
05A	2011	SN	19 Nov	26 Nov	7
Alenga	2011	JV	30 Nov	05 Dec	5
Benilde	2011	SS	23 Dec	28 Dec	5

706 **LIST OF FIGURES**

707 **Fig. 1.** Analysis domain and topography of the region (elevation scale on right). Delineation of flow  
708 regimes is based on zonal wind analyzed along blue lines at 100°E, 3-7°N and 105°E, 3-7°S. . . . . 38

709 **Fig. 2.** Cyclonic vortex genesis frequency on a 1° grid for (a) November-April and (b) May-October  
710 periods. Streamlines depict 925-850 hPa layer-average flows. Flows in (a) and (b) typify  
711 boreal winter and summer monsoon conditions, respectively. . . . . 39

712 **Fig. 3.** Monthly frequency of terrain-induced shed (top of light green bars) and non-shed (length  
713 of blue bar segments) cyclonic vortices for (a) Sumatra north (SN) and (b) Malay Peninsula  
714 (MP) regions. (c) Monthly mean zonal wind ( $\text{m s}^{-1}$ ) along 100°E (line segment shown  
715 in Fig. 1), indicating most cyclonic vortices in these regions occur in mean easterly flow  
716 during the boreal winter monsoon. Frequency of TC events originating from terrain-induced  
717 vortices shown by dark green bars. Gray shading indicates period of time with three years  
718 of data from both YOTC and DYNAMO; unshaded period has only two years of YOTC data. . . . . 40

719 **Fig. 4.** As in Fig. 3, except for (a) Sumatra south (SS) and (b) west Java (JV) regions. (c) Monthly  
720 mean zonal wind ( $\text{m s}^{-1}$ ) along 105°E (line segment shown in Fig. 1), indicating cyclonic  
721 vortices in these regions can occur during both easterly and westerly mean flow. . . . . 41

722 **Fig. 5.** (a) Tracks for all cyclonic vortices lasting longer than two days originating between 10°N  
723 and 10°S, 50°-110°E determined by the objective tracking scheme. Prominent origination  
724 sites can be seen near Sumatra, the Malay Peninsula, west Java, southern India, and Sri  
725 Lanka. (b) As in (a), except only for cyclonic vortices emanating from the four analysis re-  
726 gions: Sumatra north (SN, purple), Malay Peninsula (MP, red), Sumatra south (SS, orange),  
727 and west Java (JV, blue). . . . . 42

728 **Fig. 6.** Mean 925-850 hPa flow over Indian Ocean basin for (a) shed (40 cases) and (b) non-shed  
729 (26 cases) cyclonic vortices from region SN (black box shown) under conditions of easterly  
730 flow across northern Sumatra.  $U_N$  is average zonal flow along vertical black line shown. . . . . 43

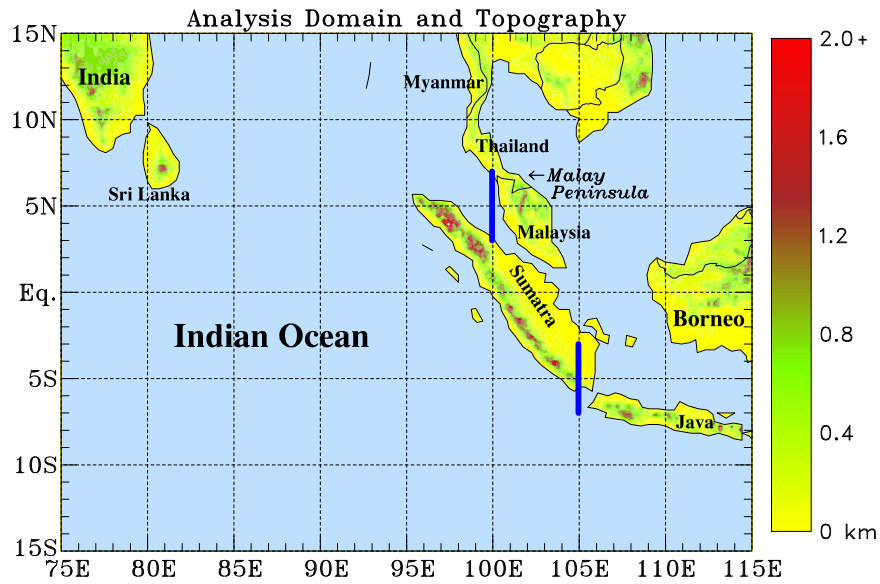
731 **Fig. 7.** Mean 925-850 hPa flow over Indian Ocean basin for shed vortices from region SS (black  
732 box shown) under conditions of (a) easterly (18 cases) and (b) westerly (7 cases) flow in the  
733 analysis region.  $U_S$  is average zonal flow along vertical black line shown. . . . . 44

734 **Fig. 8.** Mean 925-850 hPa streamlines and relative vorticity (scale at bottom) during DYNAMO  
735 (October 2011 to March 2012) for all (a) easterly and (b) westerly wind days, as determined  
736 by the zonal wind incident upon northern Sumatra. Fields shown are means for days when  
737  $|U_N| > 5 \text{ m s}^{-1}$ , where  $U_N$  is zonal wind averaged along blue line at 100°E. Panels (a) and  
738 (b) include 97 and 23 six-hourly analyses, respectively. . . . . 45

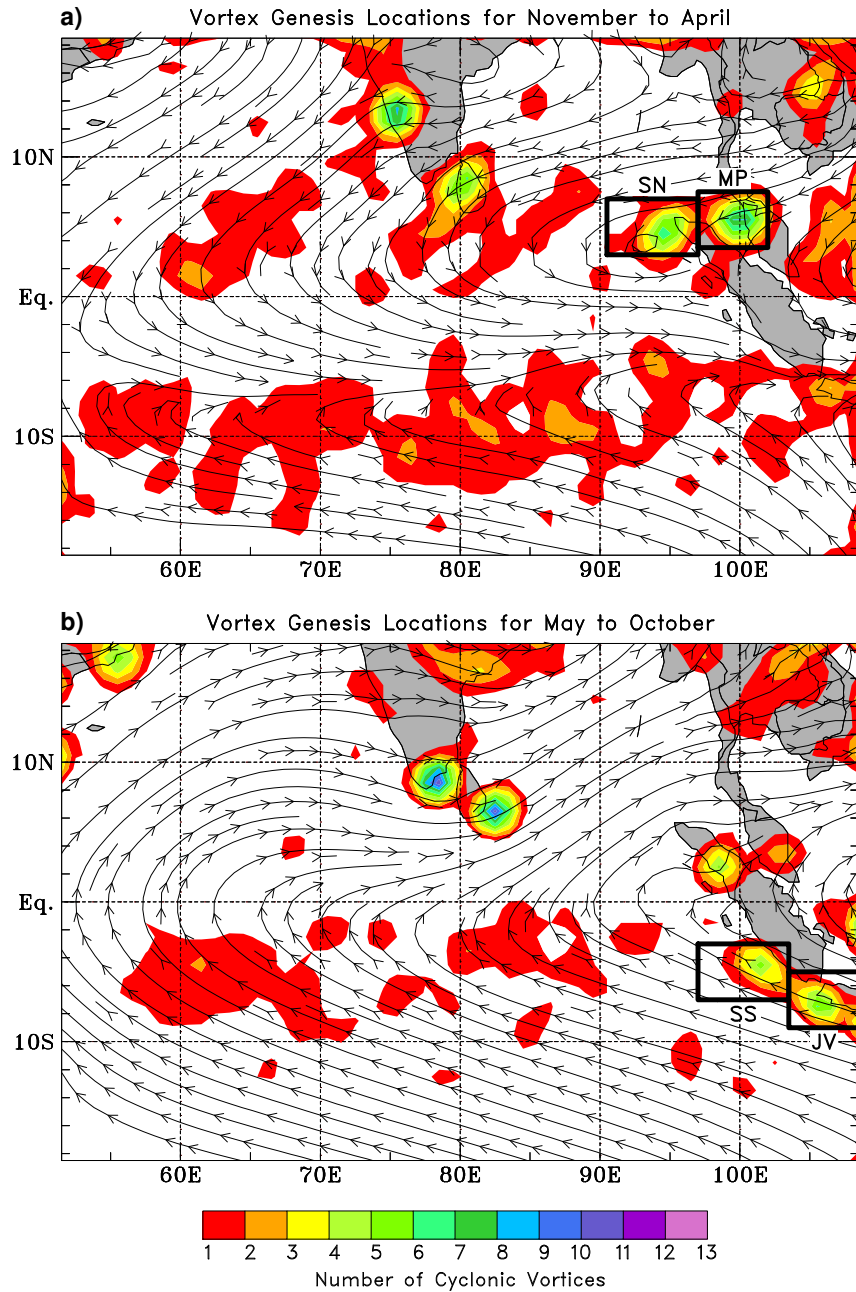
739 **Fig. 9.** Correlations between relative vorticity  $\zeta$  and zonal wind speeds  $U_N$  and  $U_S$  along northern  
740 and southern line segments, respectively, in Fig. 1 during the 2.5 years of YOTC and DY-  
741 NAMO for regions SN, MP, SS, and JV. Since portions of analysis regions include moun-  
742 tainous areas, computations are restricted only to grid points above ground level. The mag-  
743 nitudes of the correlations maximize in the lower troposphere (between 925 and 850 hPa  
744 in the north and 950 and 1000 hPa in the south), indicating the key role of topography in  
745 generating the low-level circulations. . . . . 46

746 **Fig. 10.** Relative vorticity regressed onto average zonal wind speeds  $U_N$  and  $U_S$  at 900 hPa along  
747 northern and southern line segments, respectively, in Fig. 1 during the 2.5 years of YOTC  
748 and DYNAMO for regions SN, MP, SS, and JV. Each data point consists of a concurrent

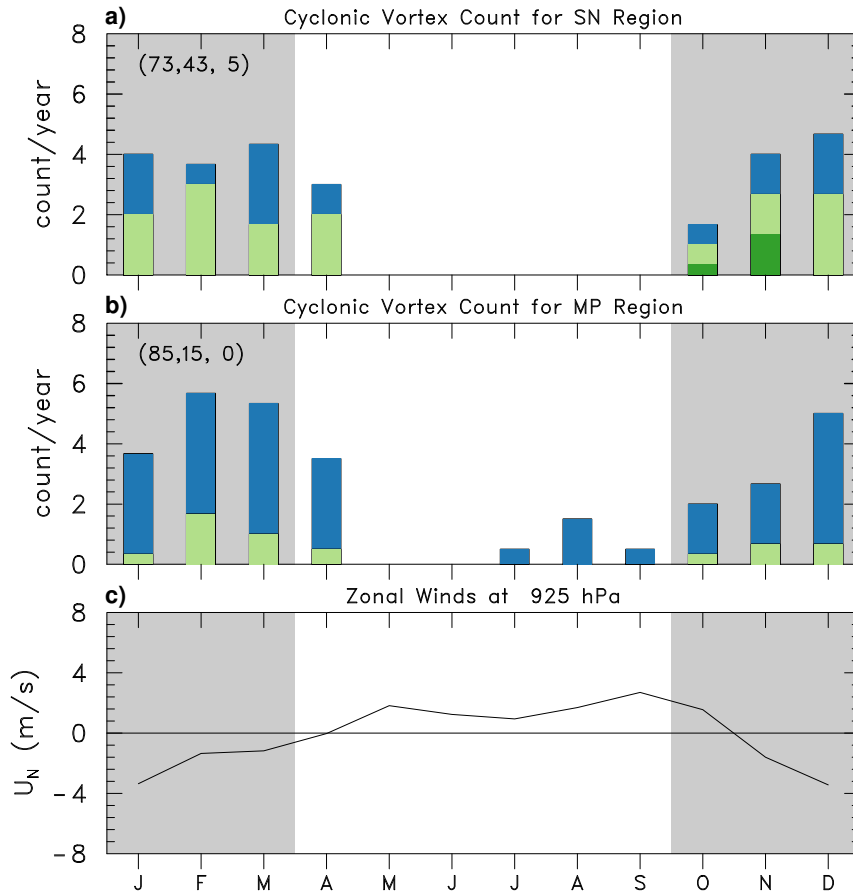
749	daily-averaged relative vorticity and zonal wind value. Solid lines are linear least-squares	
750	best fits to the data. Correlation coefficients $r$ are indicated. . . . .	47
751	<b>Fig. 11.</b> Time-longitude diagrams of daily-averaged zonal wind (color, scale at bottom) and relative	
752	vorticity (contours, plotted only for cyclonic vorticity starting at $ 1 \times 10^{-5} \text{ s}^{-1} $ with a con-	
753	tour interval of $1 \times 10^{-5} \text{ s}^{-1}$ ) for OND2008 at (a) 850 hPa, averaged over 3-7°N, and (b)	
754	925 hPa, averaged over 3-7°S. Origins of vortices that later became TCs are indicated by	
755	stars, and longitudes and days when vortices became named TCs shown by tropical cyclone	
756	symbol. Dotted lines associate which TC formed from which initial vortex. Vertical dashed	
757	lines denote longitudes of northern (a) and southern (b) tips of Sumatra. TCs may move out	
758	of the latitude averaging bands, which may account for apparent discrepancies between the	
759	“end” of a vorticity streamer and the location of tropical cyclogenesis. . . . .	48
760	<b>Fig. 12.</b> As in Fig. 11, for OND2009. . . . .	49
761	<b>Fig. 13.</b> As in Fig. 11, for OND2011. . . . .	50
762	<b>Fig. 14.</b> Tracks of Indian Ocean tropical cyclones that originated from Sumatra-region terrain-	
763	induced vortices during (a) May 2008–April 2009, (b) May 2009–April 2010, and (c) Octo-	
764	ber 2011–March 2012 time periods. Thin lines represent tracks of wake vortices before they	
765	developed into named TCs. Thick lines denote tracks of named TCs. . . . .	51
766	<b>Fig. 15.</b> 850-hPa scaled wind vectors and geopotential height anomalies (scales at bottom) for (a) 2	
767	Dec, (b) 3 Dec, (c) 4 Dec, (d) 5 Dec, (e) 6 Dec, and (f) 7 Dec 2009, showing the wake vortex	
768	precursors to TCs Cleo (labeled “C”), Ward (“W”), and David (“D”). TCs Cleo, Ward,	
769	and David were officially named storms on 7, 11, and 13 Dec, respectively. Geopotential	
770	height anomalies were calculated as the difference from a 10°S to 10°N, Indian Ocean-wide	
771	(35-120°E) geopotential height mean during OND of the same year. . . . .	52
772	<b>Fig. 16.</b> As in Fig. 15, except for (a) 19 Nov, (b) 20 Nov, (c) 21 Nov, (d) 22 Nov, (e) 23 Nov, and	
773	(f) 24 Nov 2011, showing the wake vortex precursor to TC 05A. TC 05A was an officially	
774	named storm on 26 Nov. Dark green contour is $-10 \text{ W m}^{-2}$ MJO-filtered OLR anomaly,	
775	indicating eastward progression of the MJO. . . . .	53
776	<b>Fig. 17.</b> Time-longitude diagrams of daily-averaged relative vorticity (contours, plotted only for cy-	
777	clonic vorticity starting at $1 \times 10^{-5} \text{ s}^{-1}$ with a contour interval of $1 \times 10^{-5} \text{ s}^{-1}$ ) and OLR	
778	anomalies (color, scale at bottom) filtered by (a) equatorial Rossby waves and (b) Kelvin	
779	waves for OND2011. Origins of vortices that later became TCs are indicated by stars, and	
780	longitudes and days when vortices became named TCs shown by tropical cyclone symbol.	
781	Dotted lines associate which TC formed from which initial vortex. Vertical dashed lines	
782	denote longitude of northern tip of Sumatra. . . . .	54



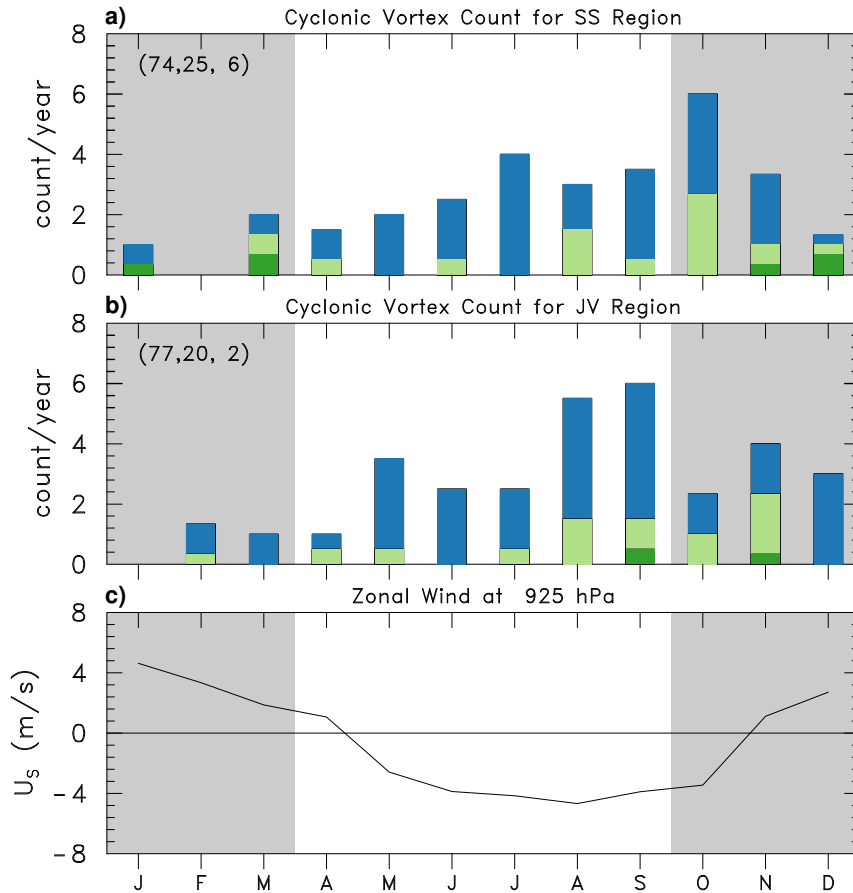
783 FIG. 1. Analysis domain and topography of the region (elevation scale on right). Delineation of flow regimes  
 784 is based on zonal wind analyzed along blue lines at 100°E, 3-7°N and 105°E, 3-7°S.



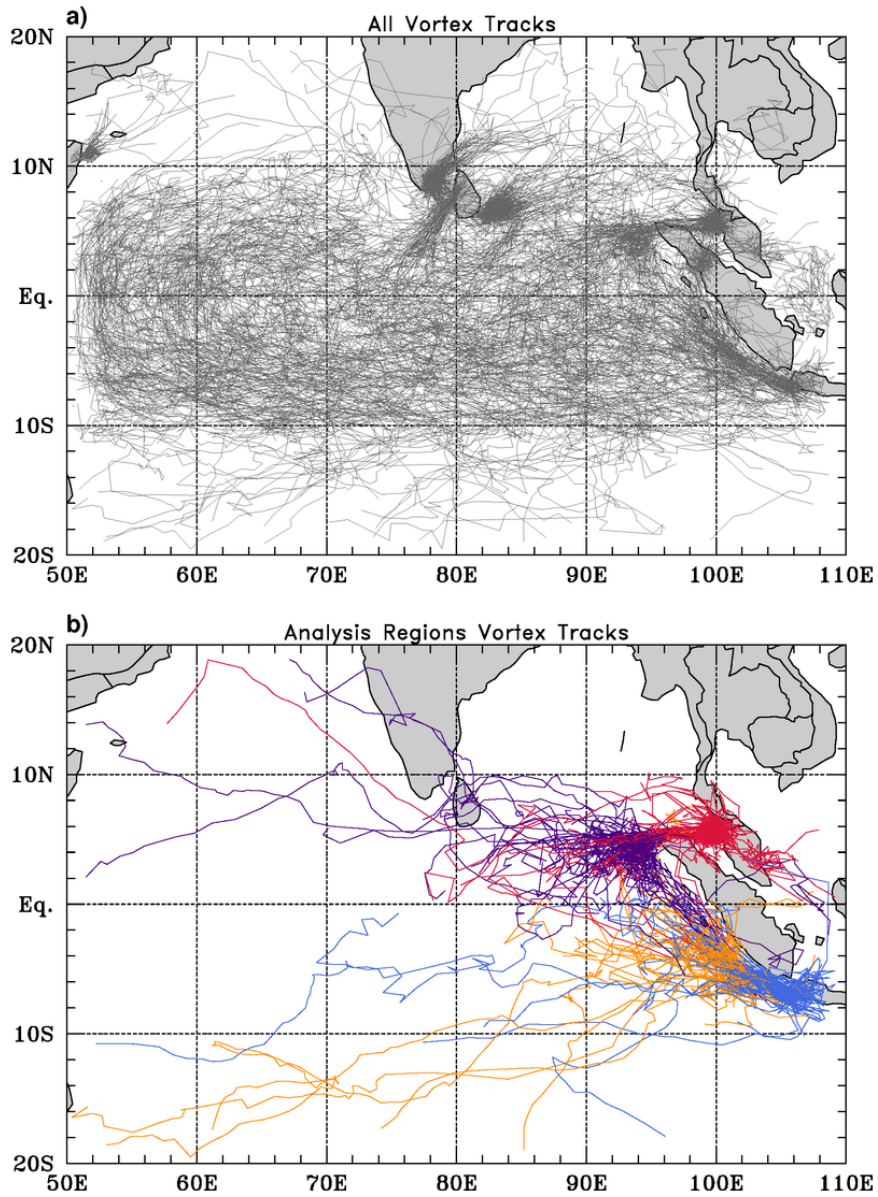
785 FIG. 2. Cyclonic vortex genesis frequency on a  $1^\circ$  grid for (a) November-April and (b) May-October periods.  
 786 Streamlines depict 925-850 hPa layer-average flows. Flows in (a) and (b) typify boreal winter and summer  
 787 monsoon conditions, respectively.



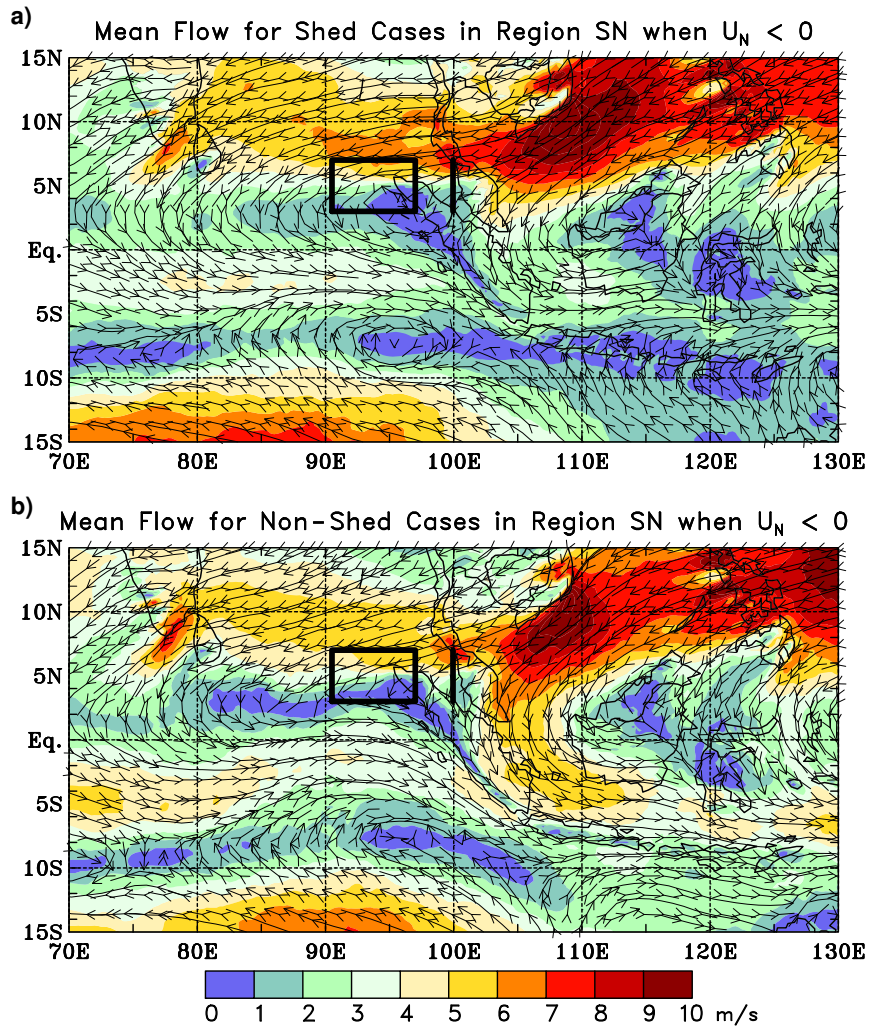
788 FIG. 3. Monthly frequency of terrain-induced shed (top of light green bars) and non-shed (length of blue  
 789 bar segments) cyclonic vortices for (a) Sumatra north (SN) and (b) Malay Peninsula (MP) regions. (c) Monthly  
 790 mean zonal wind ( $\text{m s}^{-1}$ ) along  $100^\circ\text{E}$  (line segment shown in Fig. 1), indicating most cyclonic vortices in these  
 791 regions occur in mean easterly flow during the boreal winter monsoon. Frequency of TC events originating from  
 792 terrain-induced vortices shown by dark green bars. Gray shading indicates period of time with three years of  
 793 data from both YOTC and DYNAMO; unshaded period has only two years of YOTC data.



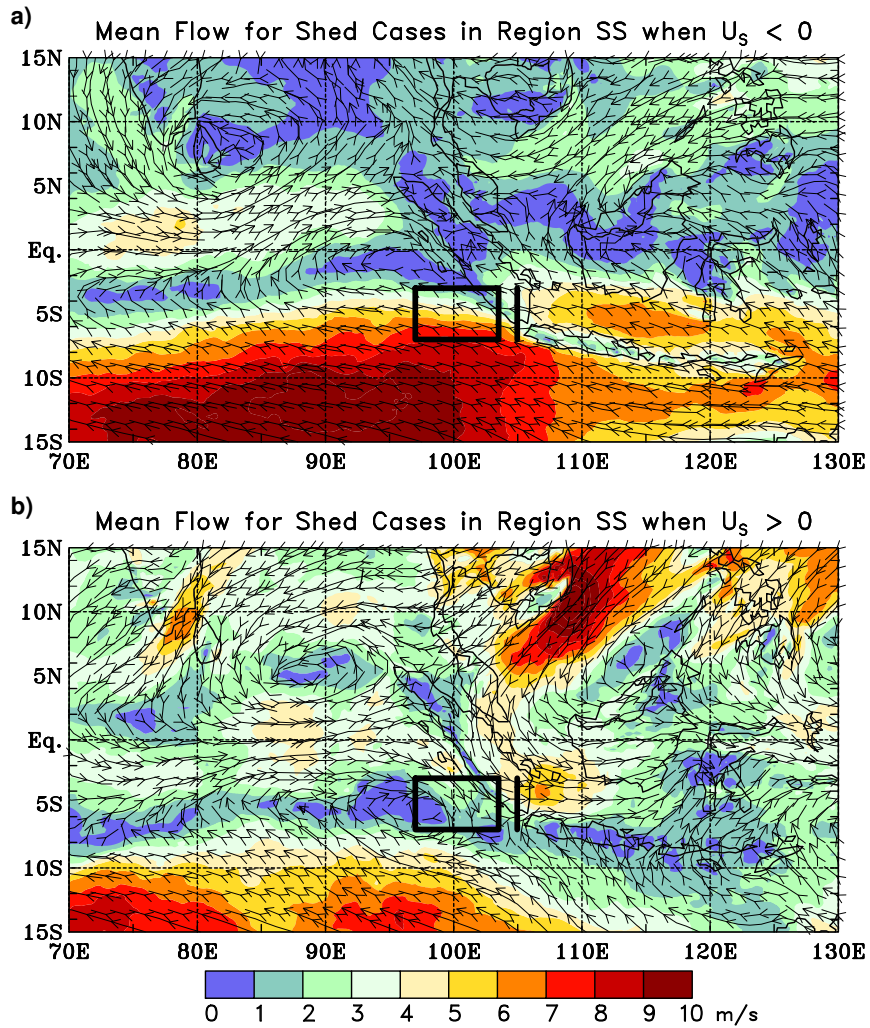
794 FIG. 4. As in Fig. 3, except for (a) Sumatra south (SS) and (b) west Java (JV) regions. (c) Monthly mean  
 795 zonal wind ( $\text{m s}^{-1}$ ) along  $105^\circ\text{E}$  (line segment shown in Fig. 1), indicating cyclonic vortices in these regions  
 796 can occur during both easterly and westerly mean flow.



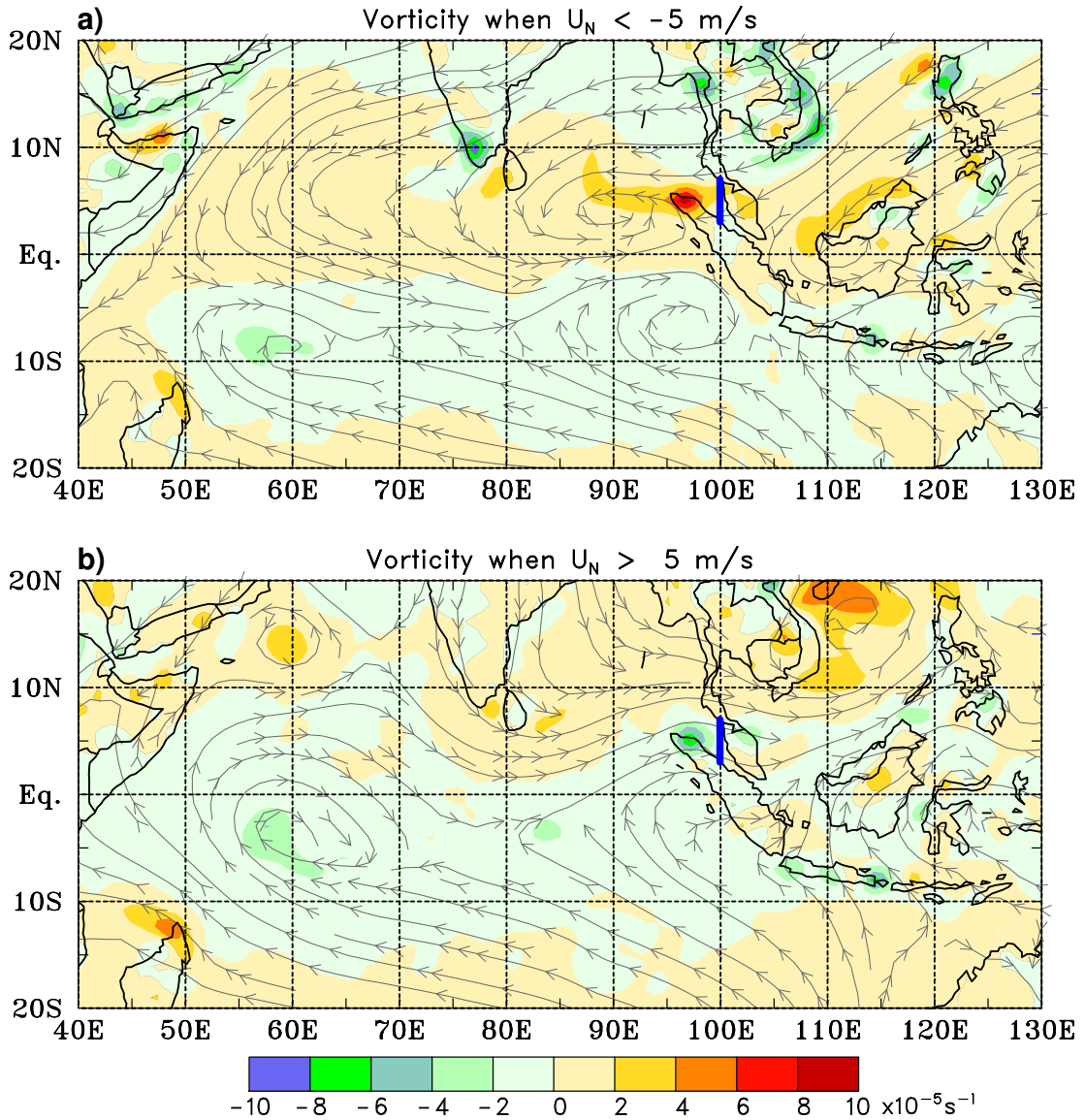
797 FIG. 5. (a) Tracks for all cyclonic vortices lasting longer than two days originating between 10°N and 10°S,  
 798 50°-110°E determined by the objective tracking scheme. Prominent origination sites can be seen near Sumatra,  
 799 the Malay Peninsula, west Java, southern India, and Sri Lanka. (b) As in (a), except only for cyclonic vortices  
 800 emanating from the four analysis regions: Sumatra north (SN, purple), Malay Peninsula (MP, red), Sumatra  
 801 south (SS, orange), and west Java (JV, blue).



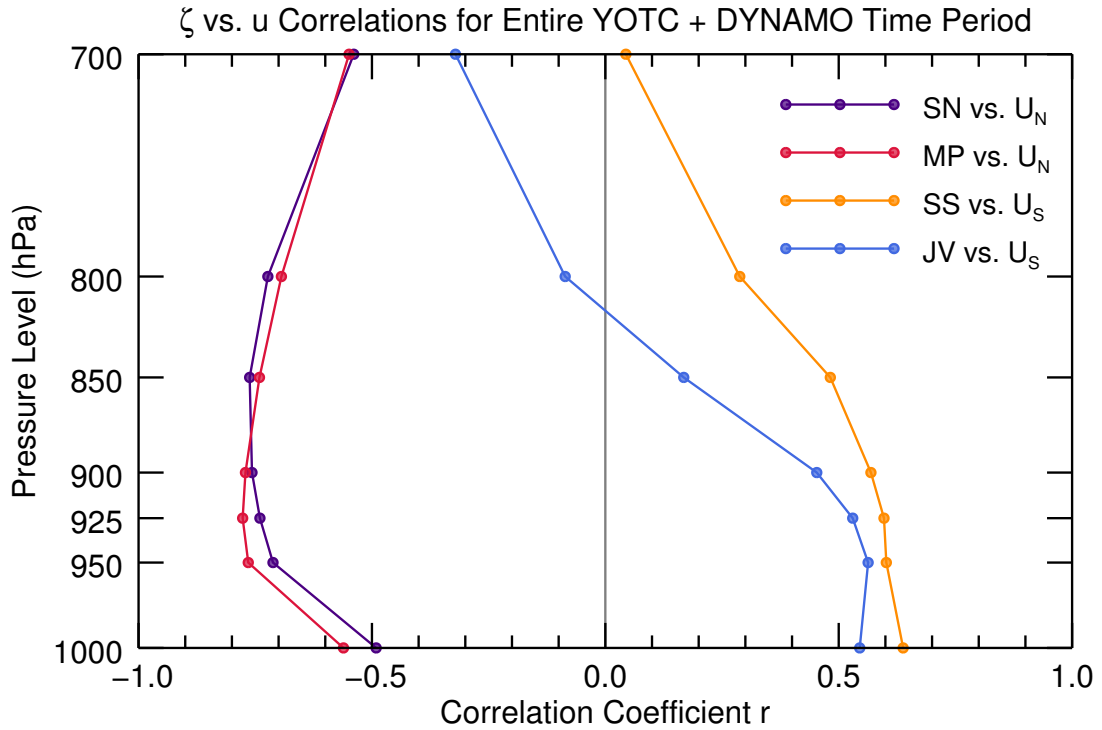
802 FIG. 6. Mean 925-850 hPa flow over Indian Ocean basin for (a) shed (40 cases) and (b) non-shed (26 cases)  
 803 cyclonic vortices from region SN (black box shown) under conditions of easterly flow across northern Sumatra.  
 804  $U_N$  is average zonal flow along vertical black line shown.



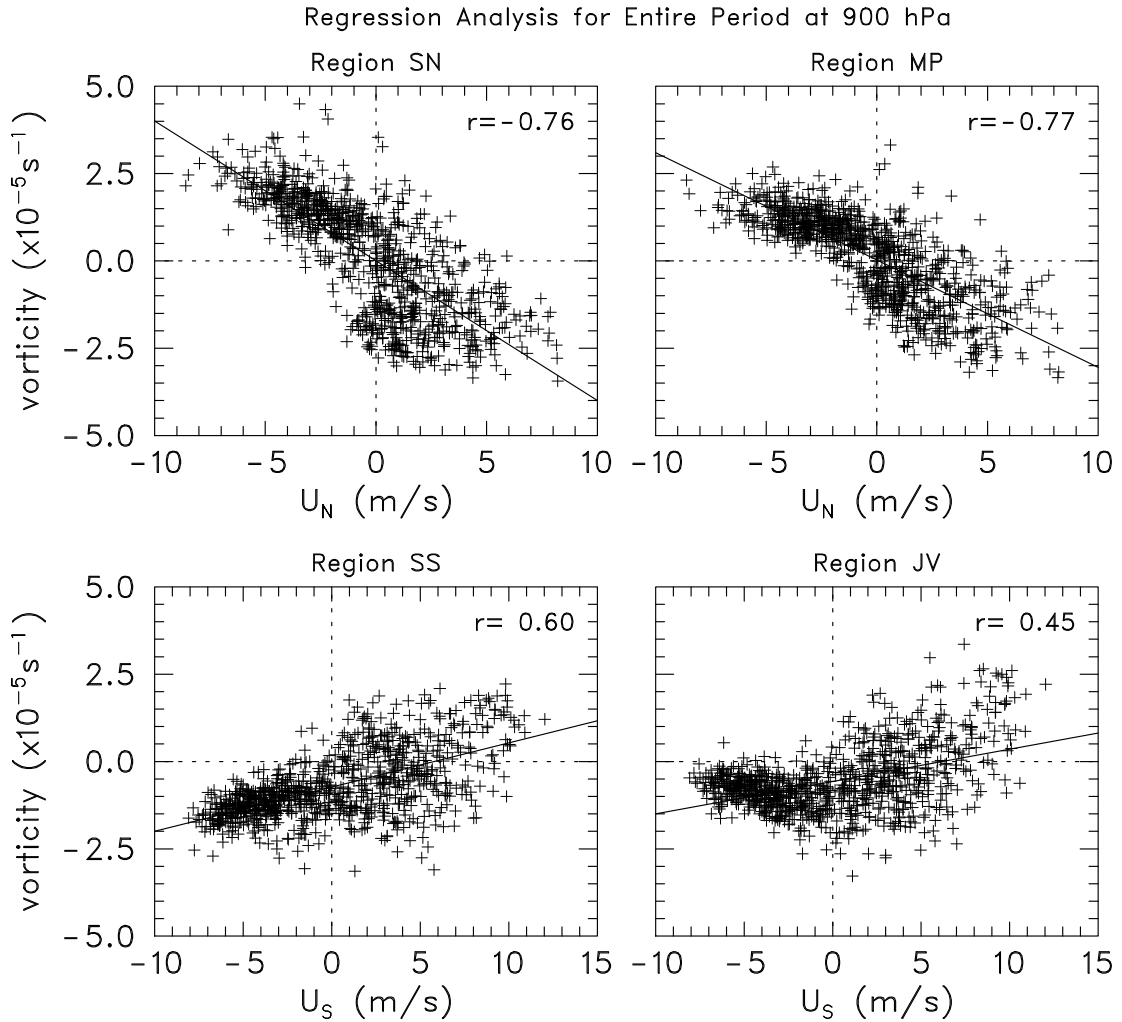
805 FIG. 7. Mean 925-850 hPa flow over Indian Ocean basin for shed vortices from region SS (black box shown)  
 806 under conditions of (a) easterly (18 cases) and (b) westerly (7 cases) flow in the analysis region.  $U_s$  is average  
 807 zonal flow along vertical black line shown.



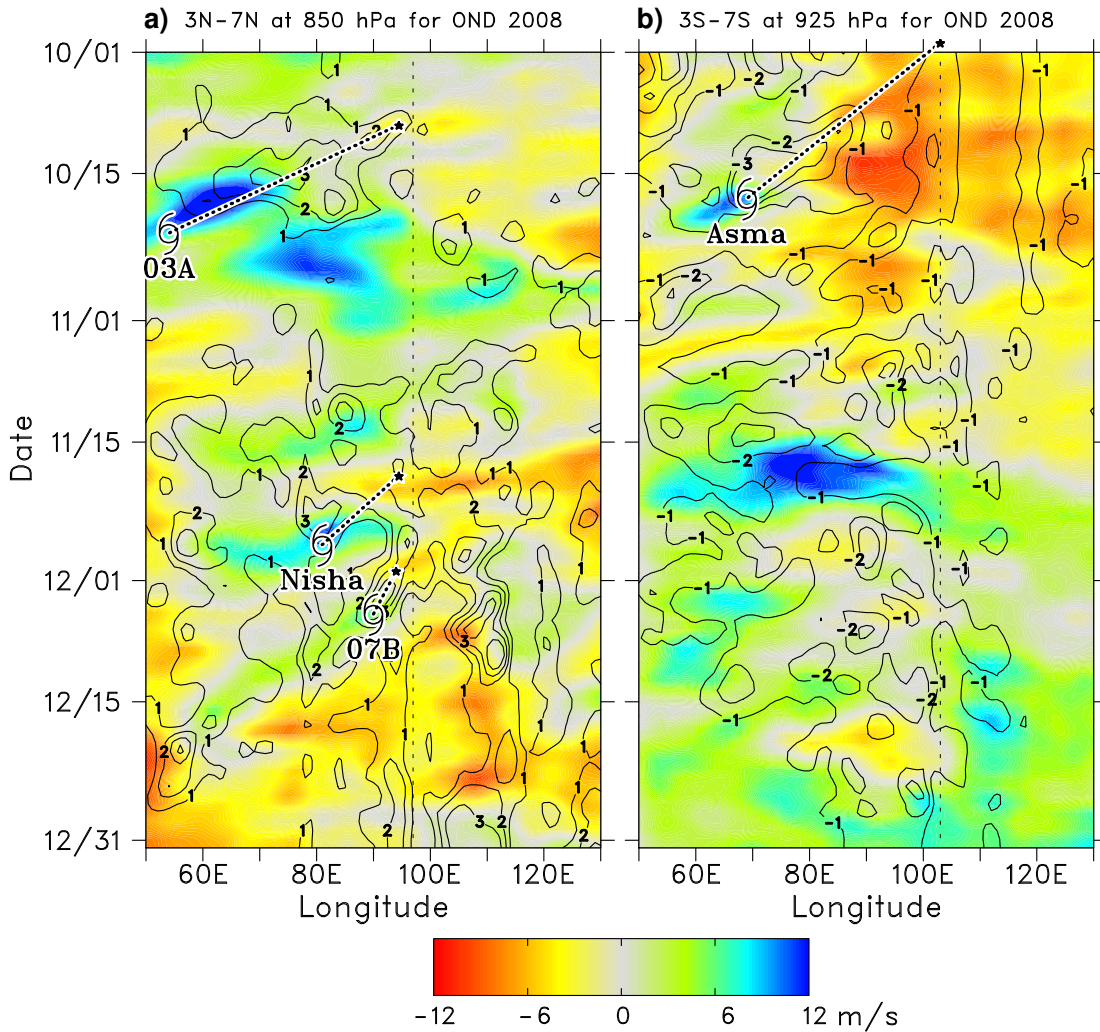
808 FIG. 8. Mean 925-850 hPa streamlines and relative vorticity (scale at bottom) during DYNAMO (October  
 809 2011 to March 2012) for all (a) easterly and (b) westerly wind days, as determined by the zonal wind incident  
 810 upon northern Sumatra. Fields shown are means for days when  $|U_N| > 5 \text{ m s}^{-1}$ , where  $U_N$  is zonal wind  
 811 averaged along blue line at  $100^\circ\text{E}$ . Panels (a) and (b) include 97 and 23 six-hourly analyses, respectively.



812 FIG. 9. Correlations between relative vorticity  $\zeta$  and zonal wind speeds  $U_N$  and  $U_S$  along northern and  
 813 southern line segments, respectively, in Fig. 1 during the 2.5 years of YOTC and DYNAMO for regions SN, MP,  
 814 SS, and JV. Since portions of analysis regions include mountainous areas, computations are restricted only to  
 815 grid points above ground level. The magnitudes of the correlations maximize in the lower troposphere (between  
 816 925 and 850 hPa in the north and 950 and 1000 hPa in the south), indicating the key role of topography in  
 817 generating the low-level circulations.



818 FIG. 10. Relative vorticity regressed onto average zonal wind speeds  $U_N$  and  $U_S$  at 900 hPa along northern  
 819 and southern line segments, respectively, in Fig. 1 during the 2.5 years of YOTC and DYNAMO for regions SN,  
 820 MP, SS, and JV. Each data point consists of a concurrent daily-averaged relative vorticity and zonal wind value.  
 821 Solid lines are linear least-squares best fits to the data. Correlation coefficients  $r$  are indicated.



822 FIG. 11. Time-longitude diagrams of daily-averaged zonal wind (color, scale at bottom) and relative vorticity  
 823 (contours, plotted only for cyclonic vorticity starting at  $|1 \times 10^{-5} \text{ s}^{-1}|$  with a contour interval of  $1 \times 10^{-5} \text{ s}^{-1}$ )  
 824 for OND2008 at (a) 850 hPa, averaged over 3-7°N, and (b) 925 hPa, averaged over 3-7°S. Origins of vortices  
 825 that later became TCs are indicated by stars, and longitudes and days when vortices became named TCs shown  
 826 by tropical cyclone symbol. Dotted lines associate which TC formed from which initial vortex. Vertical dashed  
 827 lines denote longitudes of northern (a) and southern (b) tips of Sumatra. TCs may move out of the latitude  
 828 averaging bands, which may account for apparent discrepancies between the “end” of a vorticity streamer and  
 829 the location of tropical cyclogenesis.

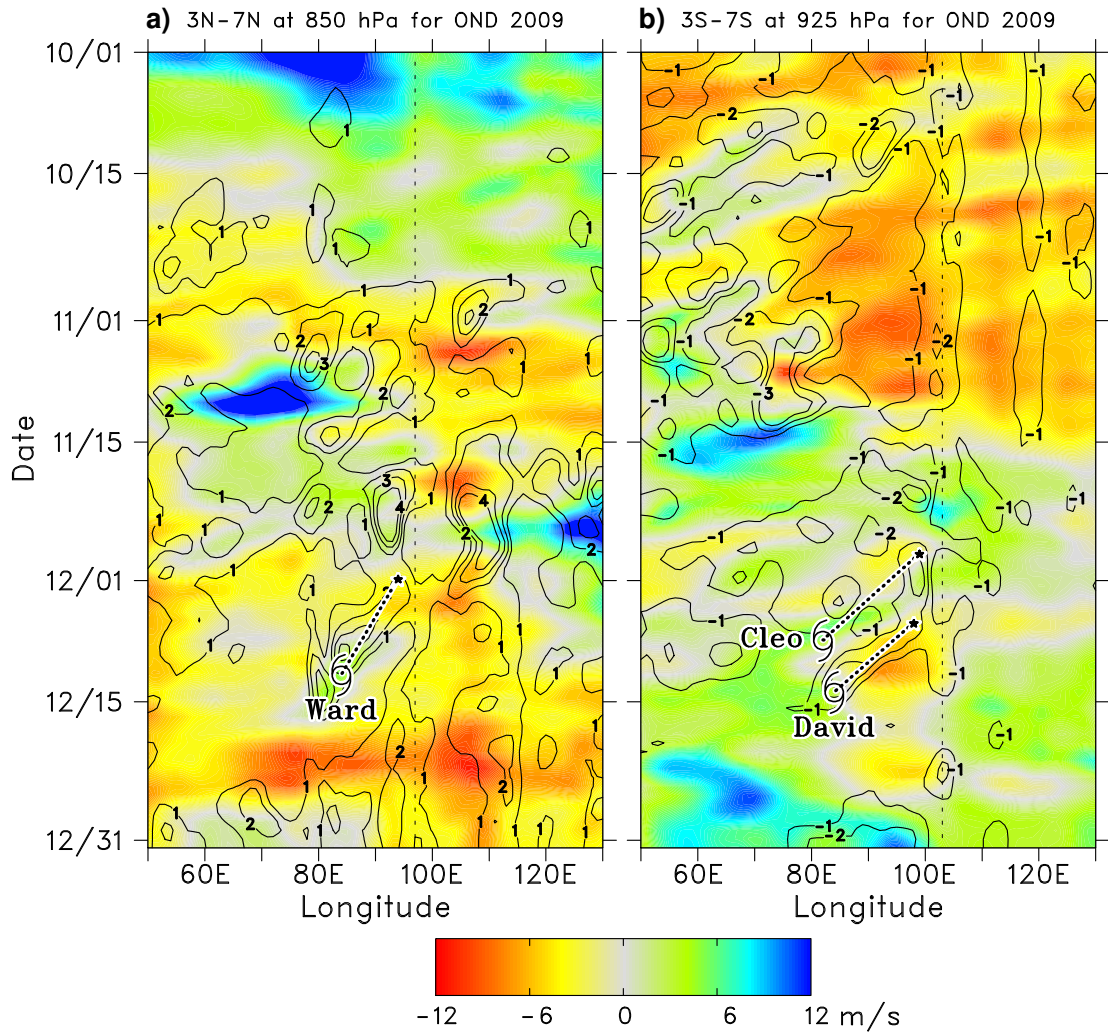


FIG. 12. As in Fig. 11, for OND2009.

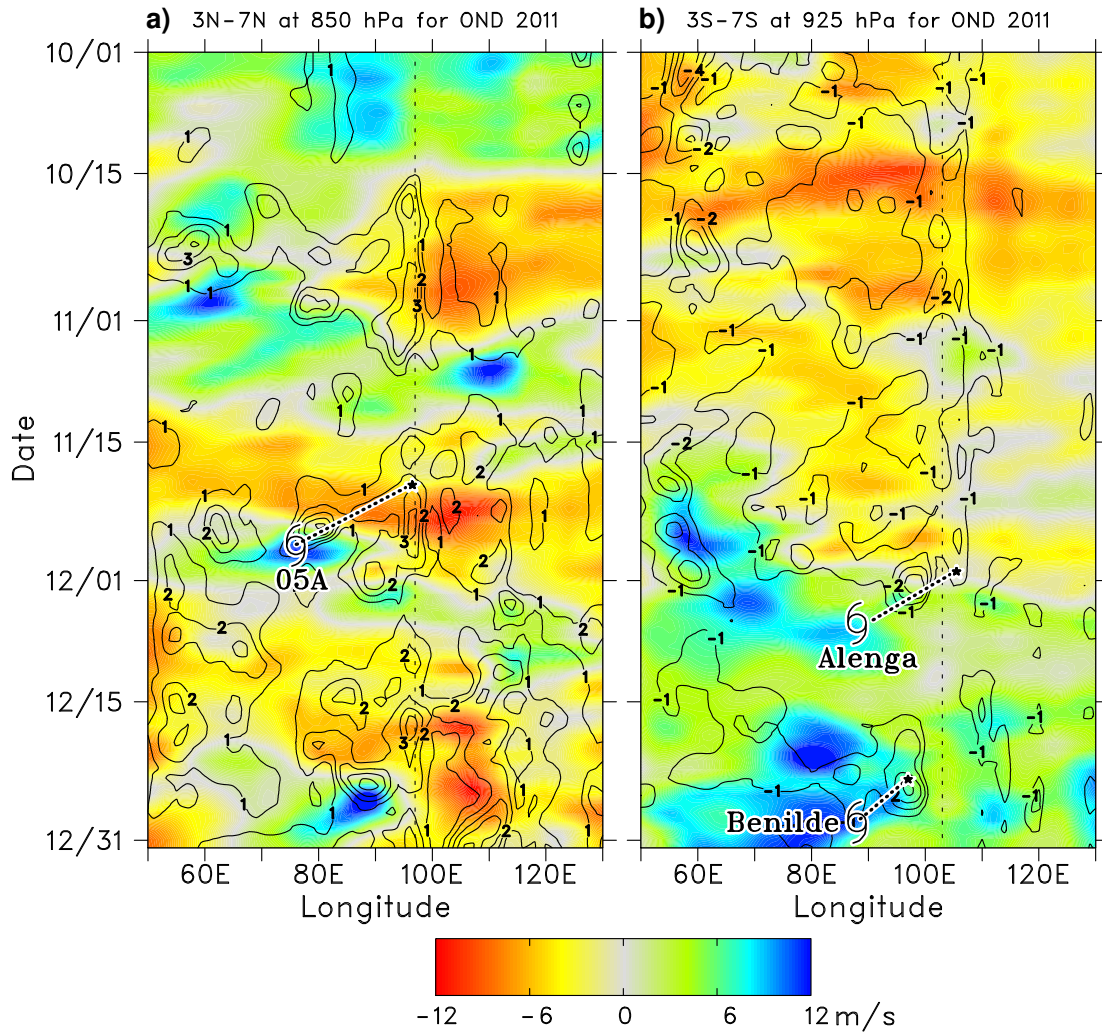
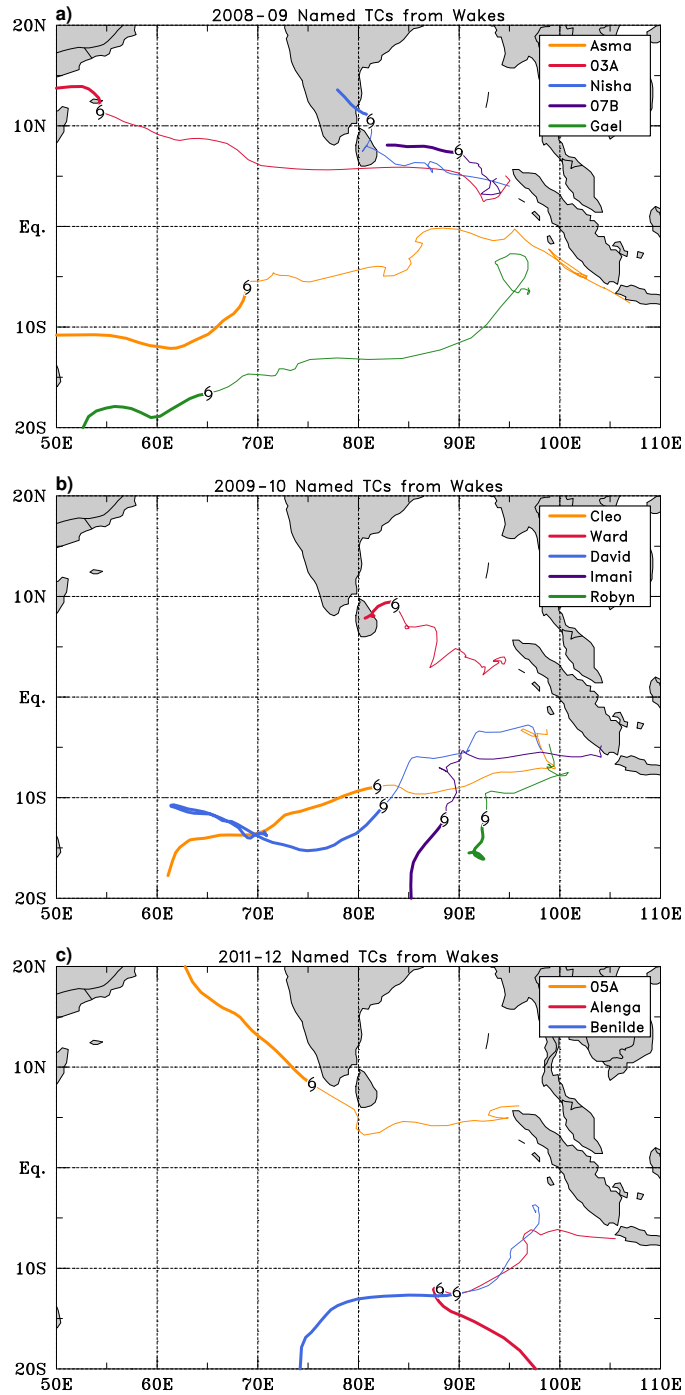
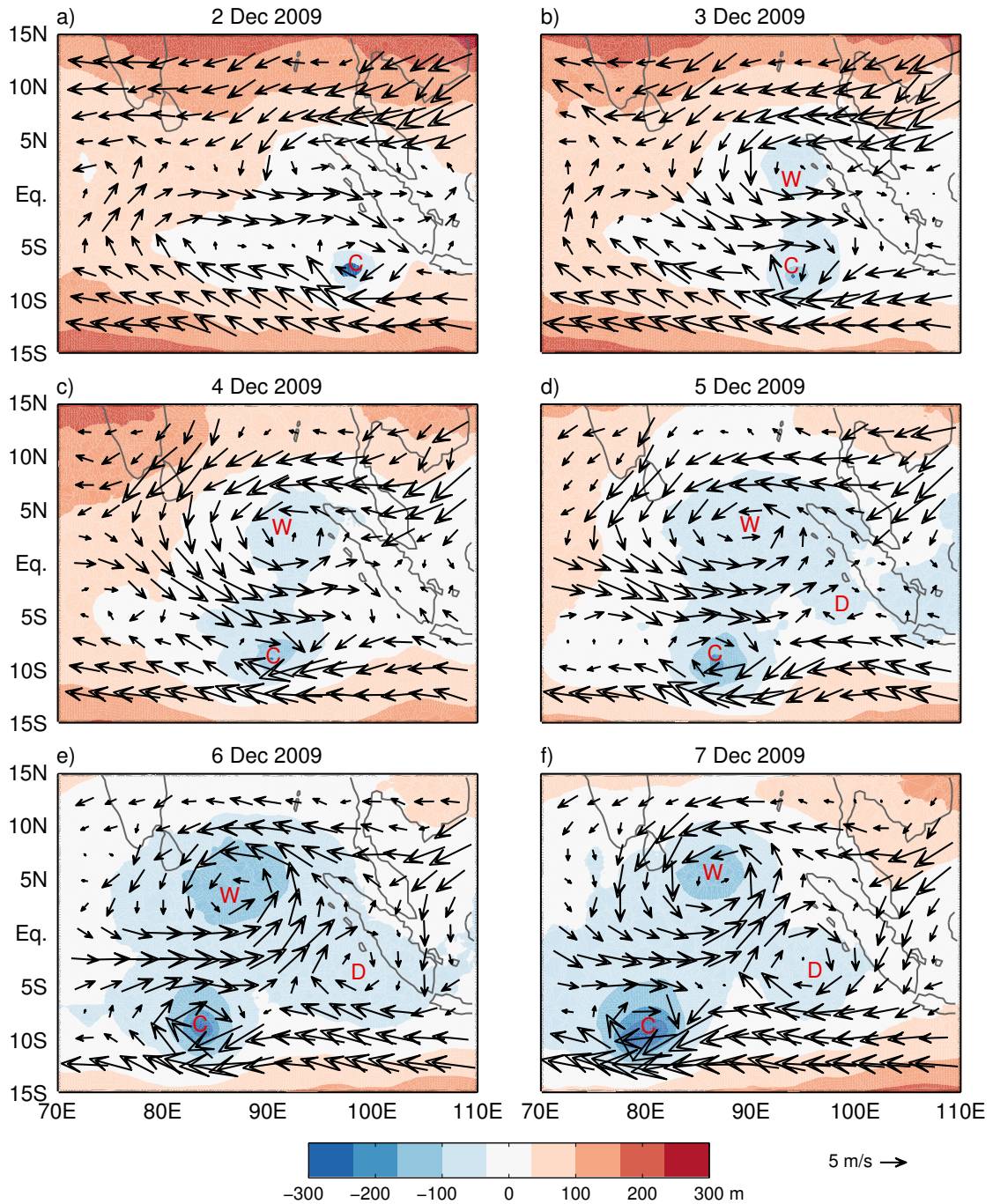


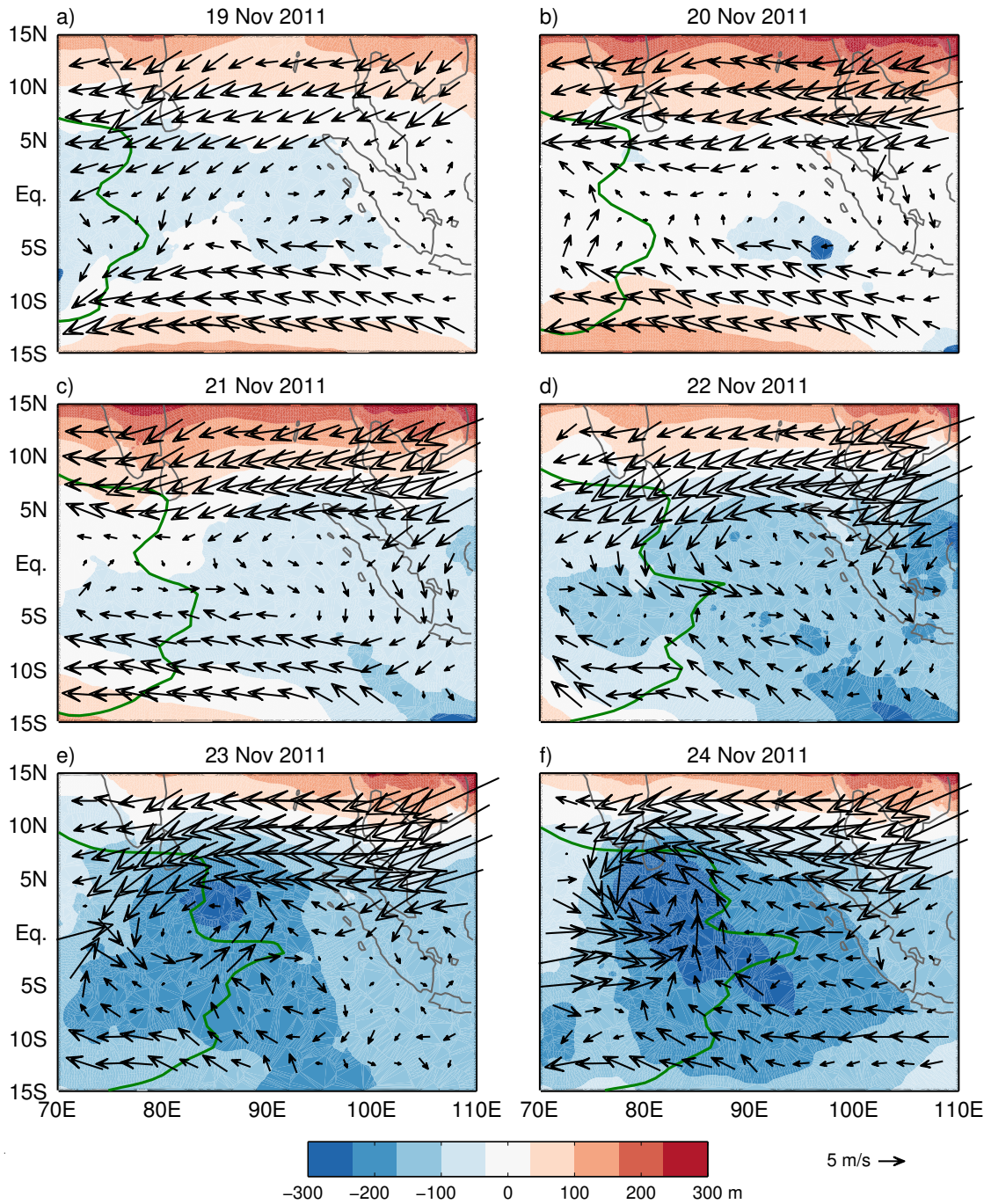
FIG. 13. As in Fig. 11, for OND2011.



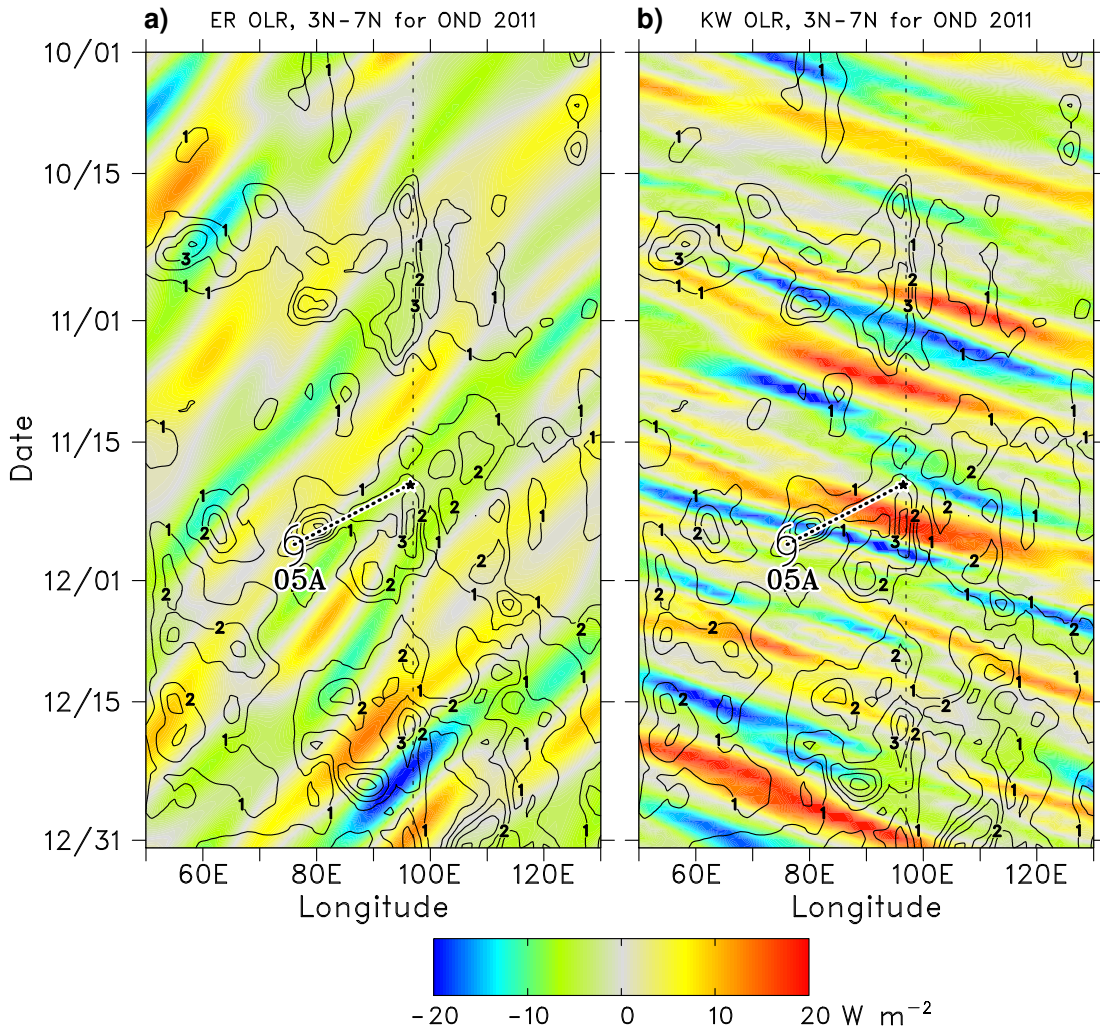
830 FIG. 14. Tracks of Indian Ocean tropical cyclones that originated from Sumatra-region terrain-induced vor-  
 831 tices during (a) May 2008–April 2009, (b) May 2009–April 2010, and (c) October 2011–March 2012 time  
 832 periods. Thin lines represent tracks of wake vortices before they developed into named TCs. Thick lines denote  
 833 tracks of named TCs.



834 FIG. 15. 850-hPa scaled wind vectors and geopotential height anomalies (scales at bottom) for (a) 2 Dec, (b)  
 835 3 Dec, (c) 4 Dec, (d) 5 Dec, (e) 6 Dec, and (f) 7 Dec 2009, showing the wake vortex precursors to TCs Cleo  
 836 (labeled “C”), Ward (“W”), and David (“D”). TCs Cleo, Ward, and David were officially named storms on 7,  
 837 11, and 13 Dec, respectively. Geopotential height anomalies were calculated as the difference from a 10°S to  
 838 10°N, Indian Ocean-wide (35-120°E) geopotential height mean during OND of the same year.



839 FIG. 16. As in Fig. 15, except for (a) 19 Nov, (b) 20 Nov, (c) 21 Nov, (d) 22 Nov, (e) 23 Nov, and (f) 24 Nov  
 840 2011, showing the wake vortex precursor to TC 05A. TC 05A was an officially named storm on 26 Nov. Dark  
 841 green contour is  $-10 \text{ W m}^{-2}$  MJO-filtered OLR anomaly, indicating eastward progression of the MJO.



842 FIG. 17. Time-longitude diagrams of daily-averaged relative vorticity (contours, plotted only for cyclonic  
 843 vorticity starting at  $1 \times 10^{-5} s^{-1}$  with a contour interval of  $1 \times 10^{-5} s^{-1}$ ) and OLR anomalies (color, scale at  
 844 bottom) filtered by (a) equatorial Rossby waves and (b) Kelvin waves for OND2011. Origins of vortices that  
 845 later became TCs are indicated by stars, and longitudes and days when vortices became named TCs shown by  
 846 tropical cyclone symbol. Dotted lines associate which TC formed from which initial vortex. Vertical dashed  
 847 lines denote longitude of northern tip of Sumatra.